

Anyonic Quantum Walks
(Research thesis)

Anyonové kvantové procházky
(Výzkumný úkol)

Václav Zatloukal¹

2010

¹Faculty of Nuclear Sciences and Physical Engineering, Czech Technical University in Prague

Abstract:

Quantum walks, the quantum analogy of classical random walks, have been studied in quantum information theory through the search for efficient new quantum algorithms. It is known that the diffusion of a quantum walker is quadratically faster compare to its classical counterpart. Here we will focus on how the quantum walk distribution can be affected by the statistical properties of a walker in two dimensional space, where not only bosons and fermions, but also anyons can appear. Exchanging two anyons can introduce phase factors or unitary matrices. This leads to a study of braid group representations, knots, links and their Jones polynomials. We consider the non-Abelian Ising anyonic model arising from the $SU(2)$ level 2 Chern-Simons theory and present the results of our numerical calculations up to 25 time steps. The diffusive behavior of an anyonic walker seems to approach (for large number of steps) the classical walker behavior.

Acknowledgement:

I would like to thank my supervisors, Dr. Jiannis Pachos, Prof. Gavin Brennen and Dr. Petr Jizba, and my colleague Lauri Lehman for introducing me into the topic and helping me understand it. I also thank Dr. Almut Beige for organizing my visit at the University of Leeds. Finally, I want to thank Andreas Kurcz, Michal Hajdusek, Tony Blake, Ville Lahtinen and all the other people from the School of Physics and Astronomy, University of Leeds for making my stay in Leeds an enjoyable and unforgettable experience.

Contents

1	Introduction and motivation	4
2	Knot theory	6
2.1	Knots in mathematics	6
2.2	Braids and the braid group	10
2.3	Jones polynomial	14
3	Anyons	17
3.1	Anyons as flux-charge composites	18
3.2	Ising anyonic model	19
4	Anyonic quantum walk on a line	26
4.1	Classical random walk	26
4.2	Quantum walk on a line	28
4.3	A walk with Ising anyons	30
4.3.1	Evaluation of the trace over the fusion space	33
4.3.2	Numerical calculation	37
5	Conclusion, discussion and outlook	41
5.1	Why the Ising walk behaves classically	41
5.2	Walks with $SU(2)$ level k anyons	42

Chapter 1

Introduction and motivation

Quantum versions of random walks came to prominence in quantum information theory through the search for efficient algorithms. Since classical random walks provide the techniques for some of the best classical algorithms, it was natural to look for a quantum equivalent. Typically, a quantum walk gives a quadratic algorithmic speed-up over classical ones [2] and for some problems an exponential speed-up is possible [3]. This is a generalization of the faster spreading behavior shown by the simplest quantum walk — a single walker on an infinite line.

Quantum walks have since found wider applications than their algorithmic origins. For example, they have been employed in modeling transport of charge or energy in biological systems [4], in physical systems to show delocalization and quantum coherence [5, 6, 7], as well as a model system interpolating between quantum and classical behavior [8]. Quantum walks have been studied theoretically on many different structures: in higher dimensions [9], under the effects of decoherence [10], with Dirac spin particles [11] and with a huge range of variations on the basic walk dynamics.

Here we focus on the question of how the quantum walk distribution can be affected by the statistical properties of the walker. Non-interacting bosons in quantum walks have effectively already been shown to have identical properties to single quantum walkers through experiments with coherent light [8, 12]. Omar *et al.* [13] studied quantum walks with two bosonic or fermionic walkers. Entanglement in the initial state of these walkers gives strikingly different behavior with respect to the standard quantum walk.

More exotic statistics than the bosonic and the fermionic can be found in two-dimensional systems where anyons can appear. Exchanging two anyons can introduce phase factors or unitary transformations. These evolutions are different representations of the braiding group. Envisioning how the quantum walks can be performed with anyons, one realizes that the problem takes the form of diffusion of a walker-anyon in the presence of other regularly arranged static anyons. In particular, we embed a one dimensional quantum walker into a two dimensional medium with a canonical line ordering of the anyons from left to right.

When the anyonic walker is moving among the static anyons, then anyonic braiding is realized evolving the overall state of the system in a non-trivial way. Hence, by considering an anyonic walker we enrich the one particle diffusion problem with statistical properties.

In order to keep track of the statistical properties of anyons, it is useful to visualize their worldlines that encode their braiding history. When the walker moves from the initial position it braids with the straight worldlines of the static anyons. Finding the walker at a certain position after a certain number of steps requires the consideration of all the different paths of the same length with the same initial and final position. This gives rise to worldline links, the complexity of which increases rapidly with respect to the number of the walker steps.

Before turning to the anyonic quantum walk we briefly introduce the standard quantum walk and the classical random walk. We also take a look at general properties of anyons and focus on a particular non-Abelian anyonic model — the Ising anyons — with fusion rules arising from the $SU(2)$ level 2 Chern-Simons theory. We will study the walk with these Ising anyons and present the results of our numerical calculations.

In the first place, however, we make an introduction into the theory of knots, links and braids since the Ising anyonic walker probability distribution, as we shall see, is expressed in terms of the Jones polynomials (or the Kauffman brackets), i.e. phenomena that appear in the knot theory, and the knowledge of the basic concepts of the knot theory will provide a useful insight.

Chapter 2

Knot theory

In this chapter we provide an introduction into the mathematical theory of knots. We talk about knot equivalency and Reidemeister moves, we introduce links (multicomponent knots) and define the linking number. We show how braids are described and how they can give rise to knots and links. Our ultimate aim is to define an important knot invariant called the Jones polynomial, since this quantity will later on be used to describe the spatial distribution of our anyonic quantum walker.

2.1 Knots in mathematics

In mathematics, knot theory is the area of topology that studies mathematical knots. While inspired by knots which appear in daily life in shoelaces and rope, a mathematician's knot differs in that the ends are joined together to prevent it from becoming undone. In precise mathematical language, a knot is an embedding of a circle S^1 in 3-dimensional Euclidean space, \mathbb{R}^3 . Thus every knot is homeomorphic to S^1 and contains no intersections. Two knots are equivalent if one can be transformed into the other via a deformation of \mathbb{R}^3 upon itself (known as an ambient isotopy); these transformations correspond to manipulations of a knotted string that do not involve cutting the string or passing the string through itself (at each moment the circle remains embedded).

The most trivial example of a knot is the unknot, shown on Fig. 2.1(a). Under an ambient isotopy it can be positioned quite differently in space (Fig. 2.1(b), (c)). All these curves, however, represent the same knot. To decide whether two curves correspond to the same knot or not is the basic problem of the knot theory. Although algorithms exist to solve this problem [17], they can be extremely time-consuming.

In order to visualize and manipulate knots it is often useful to project them onto a plane, as we have done already in Fig. 2.1, obtaining a *knot diagram*. A small change in the direction of projection will ensure that it is one-to-one with the knot in \mathbb{R}^3 except at the double points, called crossings, where the "shadow" of the knot crosses itself once transversely (see [18] for

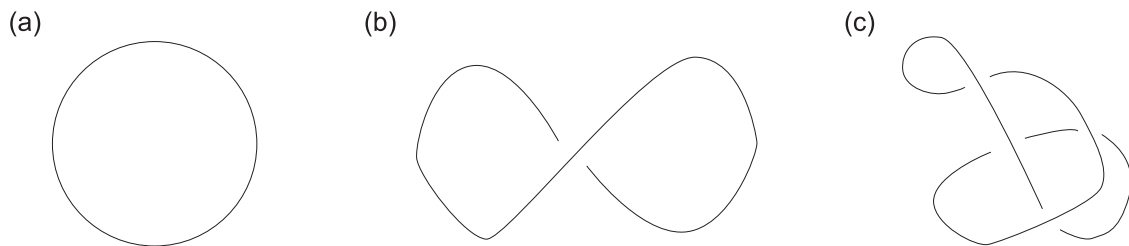


Figure 2.1: Three different projections of the same knot — the unknot.

details). At each crossing, to be able to recreate the original knot, the over-strand must be distinguished from the under-strand. This is often done by creating a break in the strand going underneath.

The knot diagram can be naturally viewed as a graph. We may perform a planar isotopy to deform the projection plane keeping the graph unchanged (Fig. 2.2). The planar isotopy

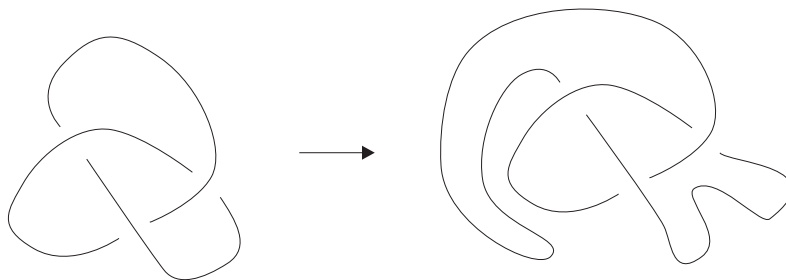


Figure 2.2: Two knot projections differing from each other by a planar isotopy represent the same knot. The knot depicted here is called the *trefoil* knot.

doesn't change the equivalence class of the corresponding knot as it can be realized (in an obvious way) by an ambient isotopy of \mathbb{R}^3 . On the other hand, ambient isotopy of the 3-space can easily change the knot diagram. Different diagrams can thus correspond to the same knot (as in Fig. 2.1) in which case we shall say that these diagrams are equivalent.

There are three basic ways of transforming a knot diagram into an equivalent one (modulo planar isotopy), named after the German mathematician Kurt Reidemeister. They are depicted in Fig. 2.3. It is understood that these moves are to be performed locally on the knot diagram and that no other strands are present (locally) than those depicted in the moves. It is apparent that any sequence of these moves only changes the knot projection, not the knot itself. A natural question to ask is: Given two equivalent knot diagrams (i.e. two projection of the same knot) does there always exist a sequence of Reidemeister moves that turns one diagram into the other? It was proved by Reidemeister in 1926 that it is indeed the case [19].

Knot theory also studies multicomponent knots, so called links. A link is an embedding of a collection of circles in \mathbb{R}^3 . Some examples of links are shown in Fig. 2.4. Knots can

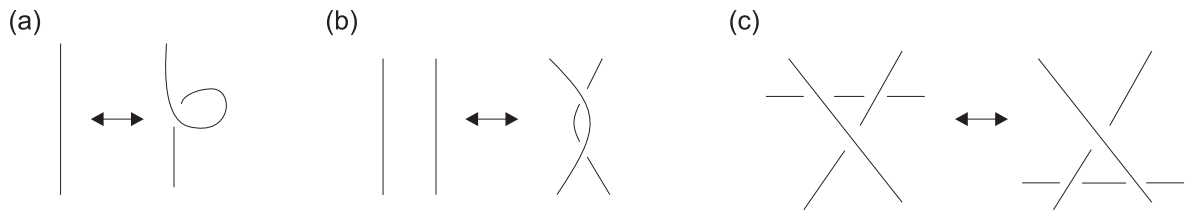


Figure 2.3: Reidemeister moves performed on a knot projection don't change the knot (they yield equivalent knot diagrams). (a) Type I (or the first) Reidemeister move twists or untwists, (b) type II (or the second) move passes one strand over another and (c) type III (or the third) move moves a strand under a crossing.

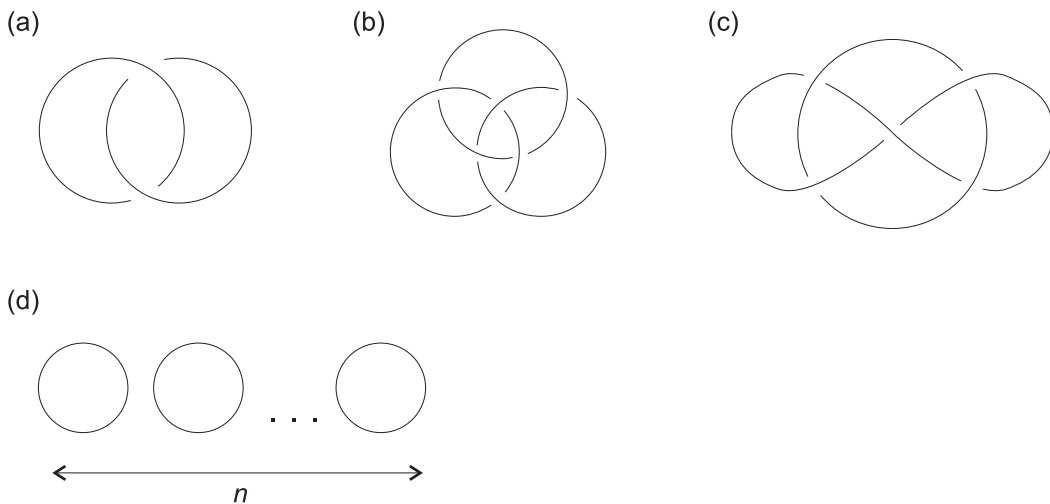


Figure 2.4: Some simple examples of links with more than one component: (a) Hopf link, (b) Borromean rings, (c) Whitehead link, (d) n -component unlink (denoted U_n).

be viewed as one-component links. Links are also treated using diagrams and, in fact, the Reidemeister's proof holds even in this more general case. We summarize:

Theorem 1 *Two knot (or link) diagrams correspond to the same knot (or link) if and only if there exists a sequence of Reidemeister moves that turns one diagram into the other.*

Let us now consider 2-component links. If α and β are the two components of a link L , and we orient them, we wish to define a new quantity - the linking number $lk(\alpha, \beta)$. The linking number should represent the number of times that one strand winds around the other. In the link diagram we focus only on those crossings that involve both components α and β and denote the set of these crossings $\alpha \cap \beta$. To each crossing $c \in \alpha \cap \beta$ we associate a sign $\epsilon(c)$ according to Fig. 2.5. The linking number between components α and β of an oriented

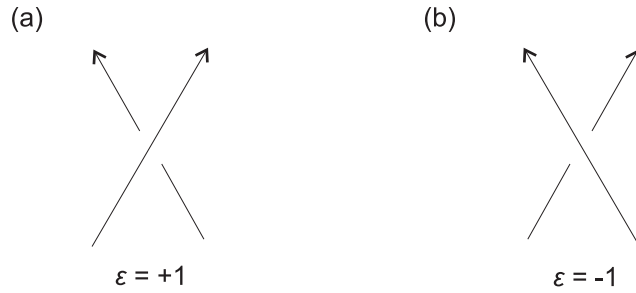


Figure 2.5: Each crossing in an oriented link projection can be assigned a sign ϵ as depicted. The assignment is done in such a way that the positive crossing ($\epsilon = +1$) can be identified using the right hand rule with the thumb following one of the arrows and the rest of fingers following the other one.

link L is defined as

$$lk(\alpha, \beta) := \frac{1}{2} \sum_{c \in \alpha \cap \beta} \epsilon(c). \quad (2.1)$$

Notice that we use a particular projection of the link in order to compute the linking number. In fact, one can show that the computed linking number will always be the same, no matter what projection of the link we use to compute it. It follows from the fact that $lk(\alpha, \beta)$ doesn't change under any of the three Reidemeister moves and the Theorem 1. Therefore the linking number is an *invariant* of an oriented link.

For example, if L is the Hopf link with its components oriented as in Fig. 2.6(a) then $lk(1, 2) = 1$. If, however, we change the orientation on one of the components (see Fig.

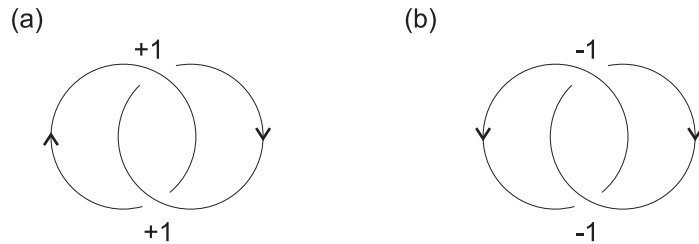


Figure 2.6: The Hopf link (in fact the simplest nontrivial example one can think of) is used here to illustrate how the linking number depends on the orientation of the link components. In the case (a) $lk(1, 2) = 1$, in the case (b) $lk(1, 2) = -1$.

2.6(b)) the linking number changes sign yielding $lk(1, 2) = -1$. In general, every change of the orientation on one of the strands α, β causes all the crossings $c \in \alpha \cap \beta$ change from positive to negative and vice versa, hence $lk(\alpha, \beta) \rightarrow -lk(\alpha, \beta)$.

If the link consists of more than two components, say $L = \alpha_1 \cup \dots \cup \alpha_n$ we may choose a pair of components and compute the linking number between these two leaving the others

out. Thus for all pairs (i, j) where $1 \leq i < j \leq n$ we get $lk(\alpha_i, \alpha_j)$. For example, in the case of the Borromean rings (see Fig. 2.4(b)) it is easily observed that all linking numbers are 0. But, of course, the Borromean rings are not the only 3-component link with linking numbers 0, 0, 0. If we put 3 disjoint circles on a plane, we have a 3-component trivial link, whose components apparently don't link at all.

The linking numbers, being invariants of an oriented link¹, allow us to sometimes distinguish links. For example, the Hopf link is certainly not the 2-component trivial link since it has non-zero linking number. On the other hand, this technique doesn't distinguish between the Borromean rings and the 3-component unlink (although they are distinct and it can be proved rigorously using the techniques of Section 2.3). The linking numbers provide only necessary condition for two links to be equivalent. This is also the case, unfortunately, for the polynomial invariants which we will introduce in Section 2.3.

2.2 Braids and the braid group

Braids are formed when n points on a horizontal plane are connected by n strings to n points on another horizontal plane, parallel to the first one, directly below the first n points. The strings are not allowed to go back upwards at any point in their travel. Two braids are considered the same (or equivalent) if one can be transformed into the other via an ambient isotopy of the space that fixes the endpoints of each string (Fig. 2.7).

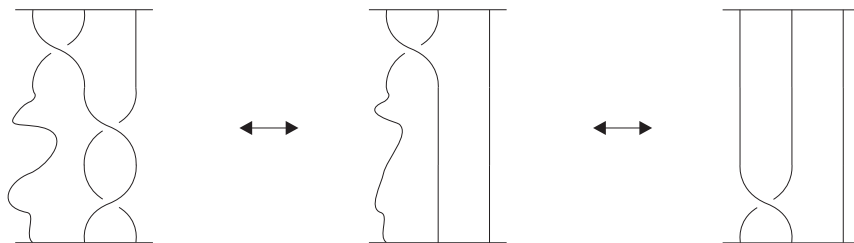


Figure 2.7: An example of equivalent braids. One can be transformed into the other via an ambient isotopy of the space that fixes the endpoints of each string.

In order to describe a given braid we define the *braid group*. The braid group B_n of n -strand braids is the group generated by $n - 1$ symbols $\sigma_1, \dots, \sigma_{n-1}$ (depicted in Fig. 2.8(a)) with the operation of concatenation (see Fig. 2.8(b)). The identity element is just "n straight lines" (Fig. 2.9(a)) and the inverse of some generator σ_j , denoted σ_j^{-1} , has contrary to σ_j the opposite type of crossing (Fig. 2.9(b)). The group relation

$$\sigma_j^{-1} \sigma_j = \sigma_j \sigma_j^{-1} = 1 \tag{2.2}$$

¹The absolute values of linking numbers $|lk(\alpha, \beta)|$ are in addition invariants of non-oriented links (they do not depend on the link components' orientations).

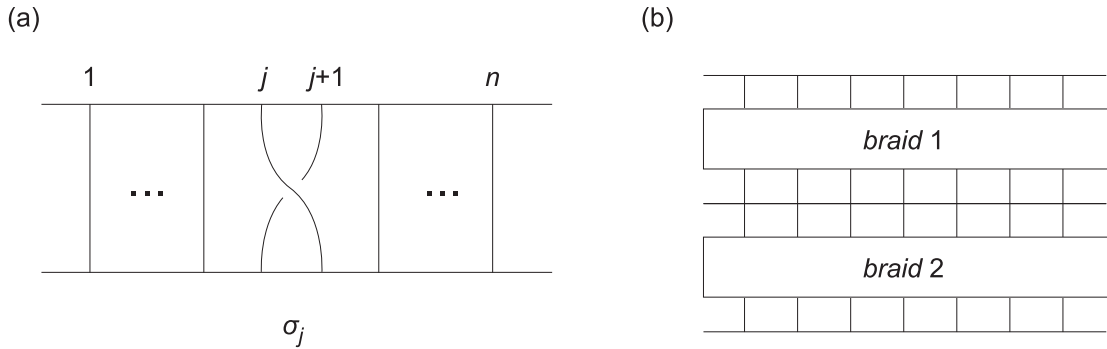


Figure 2.8: (a) The generator of the braid group B_n (j runs from 1 to $n - 1$). (b) The braid group operation of concatenation — one braid is put on top of the other and the corresponding strands are glued together.

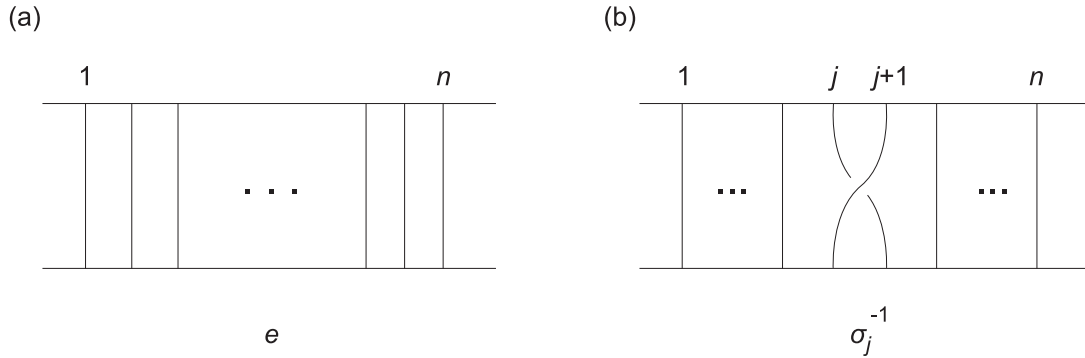


Figure 2.9: (a) The identity element in the braid group B_n . (b) The inverses of the generators σ_j of B_n .

in fact corresponds to the second Reidemeister move (recall Fig. 2.3(b)). The generators of the braid group satisfy two additional relations:

$$\sigma_i \sigma_{i+1} \sigma_i = \sigma_{i+1} \sigma_i \sigma_{i+1} \quad \text{for } i \in \{1, 2, \dots, n - 2\}, \quad (2.3)$$

$$\sigma_i \sigma_j = \sigma_j \sigma_i \quad \text{for } i, j \in \{1, \dots, n - 1\}, |i - j| \geq 2. \quad (2.4)$$

These relations are pictured in Fig. 2.10. Notice that the relation (2.3) in fact represents the third Reidemeister move (compare Fig. 2.10(a) with Fig. 2.3(c)). The relations that hold in the braid group B_n , namely (2.2), (2.3) and (2.4), guarantee that any two words in braid generators (and their inverses) represent the same braid if and only if they are the same element of B_n . This group approach to braids is due to Emil Artin [23] and therefore B_n is sometimes called Artin braid group.

Given a braid $b \in B_n$ one may form the link $(b)^{Markov}$, called the *Markov closure* of b , in a manner described by Fig. 2.11(a). A result of J. Alexander on the other hand asserts that

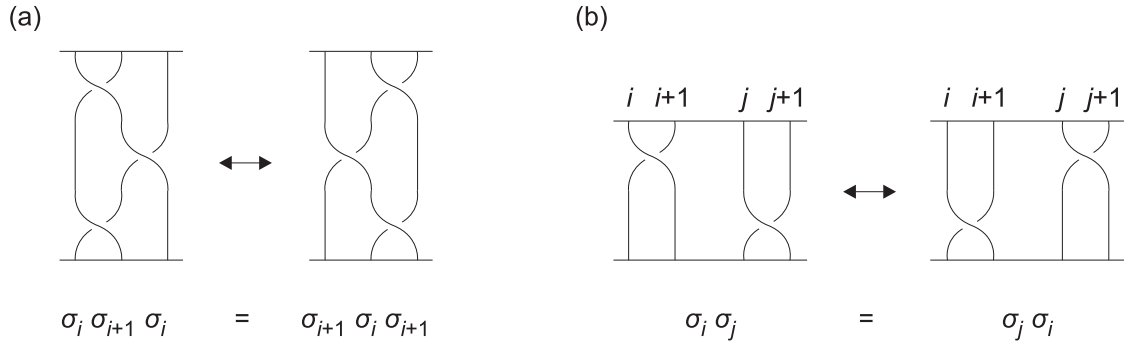


Figure 2.10: The braid group relations: (a) represents the relation 2.3 and (b) represents the relation 2.4. The braid on the left hand side is the same as that on the right hand side.

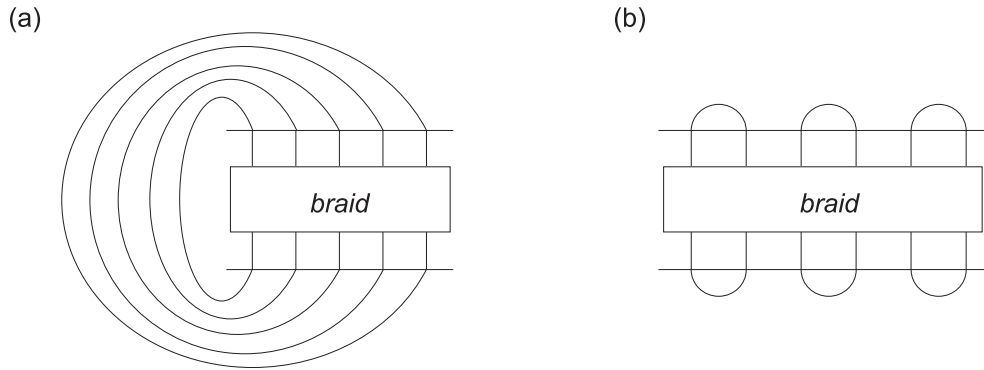


Figure 2.11: How to turn a braid into a link? Two of many imaginable ways are presented here: (a) the Markov closure, (b) the Plat closure.

for any link L there exists a braid b such that $L = (b)^{Markov}$.² The proof can be found in [15]. As an exercise, check that for $\sigma_1^2 \in B_2$ one obtains

$$(\sigma_1^2)^{Markov} = Hopf \text{ link} \quad (2.5)$$

and that the braidword $(\sigma_1^{-1} \sigma_2 \sigma_1^{-1} \sigma_2 \sigma_1^{-1} \sigma_2) \in B_3$ yields

$$(\sigma_1^{-1} \sigma_2 \sigma_1^{-1} \sigma_2 \sigma_1^{-1} \sigma_2)^{Markov} = Borromean \text{ rings}. \quad (2.6)$$

The Markov closure is not the only way how to construct links from braids. Later on in this text we will also make use of the *Plat closure* which can be applied to any braids with even number of strands. It is described by Fig. fig:braids-closures(b). Note that for any $b \in B_n$ there exist $\tilde{b} \in B_{2n}$ such that $(b)^{Markov} = (\tilde{b})^{Plat}$. Fig. 2.12 shows how \tilde{b} can be constructed.

²Here b is not unique. For example, for the braid $\sigma_1 b \sigma_1^{-1}$ we obtain the same link: $(b)^{Markov} = (\sigma_1 b \sigma_1^{-1})^{Markov}$.

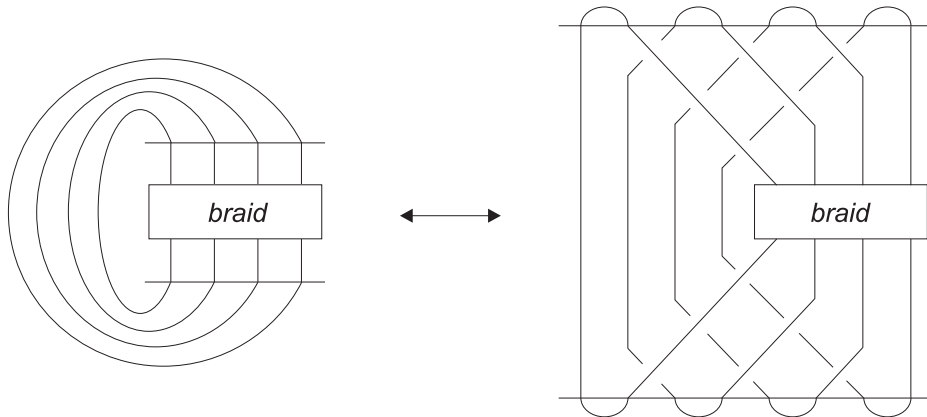


Figure 2.12: The link that is obtained by Markov closing a braid on n strands can be as well obtained by Plat closing the corresponding braid on $2n$ strands.

At the end of this section let's look at the braid group from a rather different angle. Consider n indistinguishable particles in a plane (Fig. 2.13). The configuration space of this

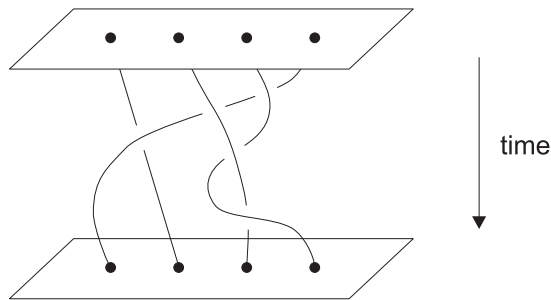


Figure 2.13: Four indistinguishable particles in a plane evolving in time. As they move around one another, the particles' worldlines in the 2+1 dimensional spacetime constitute a braid (provided that the initial and the final configuration is the same). The braid group B_4 is the fundamental group of the space of four indistinguishable particles.

physical system is

$$X = (\mathbb{C}^n \setminus \Delta) / S_n, \quad (2.7)$$

where $\Delta = \{(z_1, \dots, z_n) \in \mathbb{C}^n \mid z_i = z_j \text{ for some } i < j\}$ and S_n is the symmetric group on a set of n elements. As the particles move around in the plane, their worldlines trace curves in the 2 + 1 dimensional spacetime as depicted in Fig. 2.13. The braid group B_n is then the fundamental group of the space X , i.e.

$$B_n = \pi_1(X). \quad (2.8)$$

2.3 Jones polynomial

The Jones polynomial $V_L(t)$ is a Laurent polynomial in the variable \sqrt{t} which is defined for every oriented link L . The original definition via von Neumann algebras was given by Jones in [22]. We shall not discuss this original definition as the theory involved exceeds the scope of this thesis. Instead we present two simple recipes how to calculate the Jones polynomial.

The most elementary way to calculate $V_L(t)$ is to use the *skein relation*

$$\frac{1}{t}V_{L_+} - tV_{L_-} = \left(\sqrt{t} - \frac{1}{\sqrt{t}}\right)V_{L_0} \quad (2.9)$$

which holds for any 3 oriented links having diagrams which are identical except near one crossing where they differ as shown in Fig. 2.14. Two additional axioms are needed:

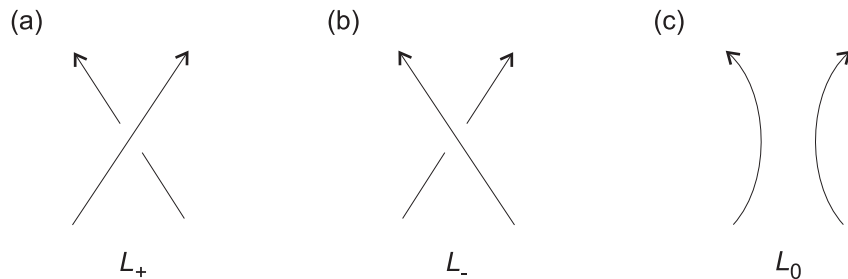


Figure 2.14: The links L_0 , L_+ and L_- are identical except near one crossing. The skein relation (2.9) is then used to calculate the Jones polynomial.

- If L is ambient isotopic to L' , i.e. L and L' are in fact the same link, then $V_L(t) = V_{L'}(t)$.
- For $L =$ "1-component unlink" we define $V_L(t) = 1$.

Notice that by appropriate change of crossings in the knot projection any knot can be reduced to the unknot. Consider, for example, a knot depicted in Fig. 2.15(a) and choose the "starting" point. Now, by appropriate change of crossings in the knot diagram (Fig. 2.15(b)) we can achieve that as we traverse the knot, viewed from the side, we decrease the "z-coordinate" until we get close enough to the starting point (see Fig. 2.15(c)). Now we only have to "climb" back to the starting point. It is clear, using the side view, that the resulting knot is the unknot. Similarly any link can be reduced to an n -component unlink U_n . But how do we compute $V_{U_n}(t)$?

Let's take a link L_0 containing two disjoint parts L and U_1 where L is an arbitrary oriented link and U_1 is the oriented unknot (see Fig. 2.16(a)). In order to use the skein relation (2.9) we find L_- and L_+ (Fig. 2.16(b), (c)). Applying the first Reidemeister move (recall the definition from Fig. 2.3(a)) we realize that $L_- = L_+ = L$. The skein relation (2.9) then reads

$$\frac{1}{t}V_L - tV_L = \left(\sqrt{t} - \frac{1}{\sqrt{t}}\right)V_{L \cup U_1} . \quad (2.10)$$

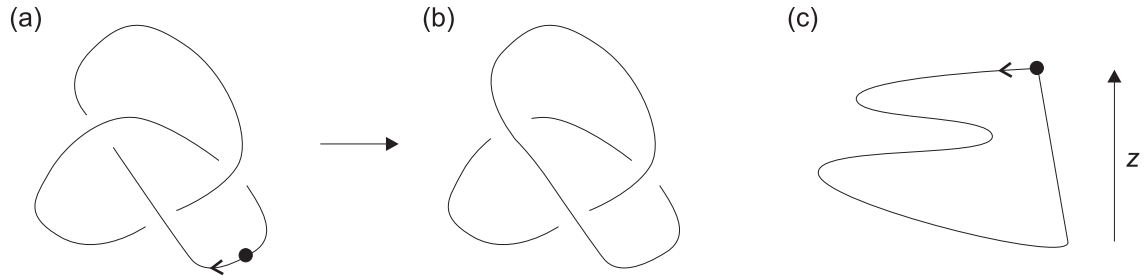


Figure 2.15: Any knot can be unknotted by appropriate change of crossings in the knot projection. We show an example of the trefoil knot which gets unknotted after one change already ((a)→(b)). The side view (c) clarifies the unknottedness of the knot.

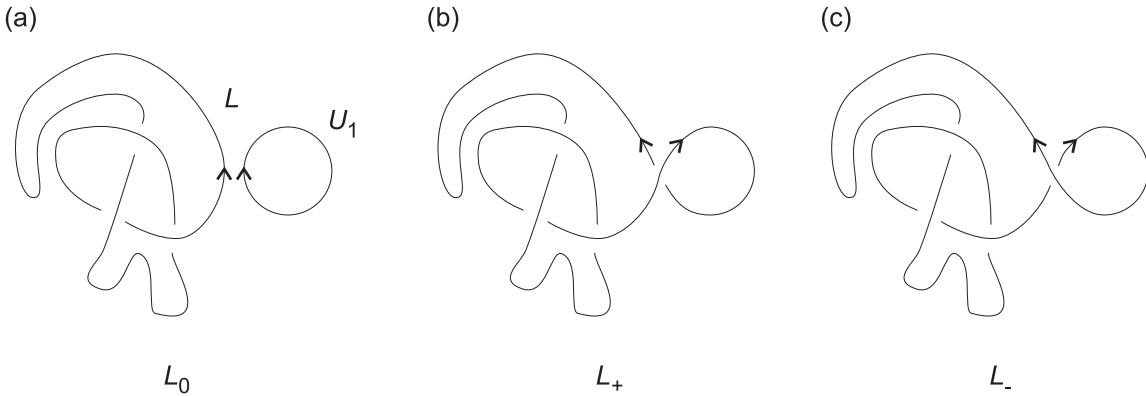


Figure 2.16: A special choice of L_0 is made. In (a), L is an arbitrary oriented link. One can see from (b) and (c) that the corresponding links L_+ and L_- are equal to L .

Thus for any oriented link L we obtain the identity

$$V_{L \cup U_1}(t) = -\left(\frac{1}{\sqrt{t}} + \sqrt{t}\right)V_L(t) , \quad (2.11)$$

which can be iterated for $L = U_n$ to yield

$$V_{U_n}(t) = \left(-\frac{1}{\sqrt{t}} - \sqrt{t}\right)^{n-1} V_{U_1}(t) = \left(-\frac{1}{\sqrt{t}} - \sqrt{t}\right)^{n-1} . \quad (2.12)$$

Now we know how to calculate the Jones polynomial for an arbitrary oriented link and we can find that, for example, for the Hopf link

$$V_{\text{Hopf link}} = -\sqrt{t}(1+t^2) . \quad (2.13)$$

Another skein-like way to calculate the Jones polynomial was found by Kauffman in [24]. This time begin with an unoriented link diagram of a link L . The Kauffman bracket

polynomial $\langle L \rangle (A)$ of such a diagram is calculated using the following three rules:

$$\langle \bigcirc \rangle = 1 , \quad (2.14)$$

$$\left\langle \begin{array}{c} \diagup \\ \diagdown \end{array} \right\rangle = A \left\langle \begin{array}{c} \diagdown \\ \diagup \end{array} \right\rangle + A^{-1} \left\langle \begin{array}{c} \frown \\ \smile \end{array} \right\rangle , \quad (2.15)$$

$$\langle \bigcirc \cup L' \rangle = (-A^2 - A^{-2}) \langle L' \rangle , \quad (2.16)$$

where L' is an arbitrary non-empty link projection and L' and \bigcirc are disjoint. The $\langle \cdot \rangle$ notation means that the relation may be applied to that part of the link diagrams inside the bracket, the rest of the diagrams being identical.

Furthermore let's define the *writhe* of an oriented link diagram L :

$$w(L) = \sum_c \epsilon(c) , \quad (2.17)$$

where the sum runs over all crossings c in the link diagram L and the crossing sign $\epsilon(c)$ has been defined earlier in the Fig. 2.5.

It was proved by Kauffman in [24] that the Jones polynomial of an oriented link L is given by the formula

$$V_L(t) = V_L(A^{-4}) = (-A)^{-3w(L)} \langle L \rangle (A) . \quad (2.18)$$

The definitions (2.14–2.16) and (2.17) guarantee that the Jones polynomial defined via (2.18) is indeed an invariant of ambient isotopies.³

The formula (2.18) has some advantages over the approach via (2.9). It makes clear how the orientation of the link components affects the resulting Jones polynomial — one only needs to calculate the writhe $w(L)$ which is an easy task. Also, this method for calculating $V_L(t)$ is very concrete and leads to the goal straightly since (2.15) allows us to eliminate every crossing, thus yielding a sum of diagrams containing unknotted disjoint loops only. Contributions of these diagrams are then easily calculated using the rules (2.14) and (2.16).⁴

You may wish to use this method to verify the result (2.13). In the case of the Hopf link $w(L) = \pm 2$ depending on the orientation of the components of the Hopf link and the Kauffman bracket $\langle L \rangle (A) = -A^4 - A^{-4}$. Thus (2.18) yields

$$V_{\left\langle \begin{array}{c} \curvearrowright \\ \curvearrowleft \end{array} \right\rangle} (t) = -\sqrt{t}(1 + t^2) \quad (2.19)$$

and

$$V_{\left\langle \begin{array}{c} \curvearrowleft \\ \curvearrowright \end{array} \right\rangle} (t) = -\frac{1}{\sqrt{t}}(1 + \frac{1}{t^2}) . \quad (2.20)$$

³This essential property is thus a consequence of the Kauffman's definition whereas in the approach via the skein relation (2.9) the invariance under ambient isotopies was one of the defining axioms.

⁴Still, however, the task of calculating $V_L(t)$ is exponentially hard in the number of crossings.

Chapter 3

Anyons

A central theme of quantum theory is the concept of indistinguishable particles. For example, all electrons in the world are exactly alike. Therefore, for a system with many electrons, an operation that exchanges two of the electrons (swaps their positions) is a symmetry — it leaves the physics unchanged. This symmetry is represented by a unitary transformation acting on the many-electron wave function.

For the indistinguishable particles in three dimensional space that we normally talk about in physics, particle exchanges are represented in two distinct ways. If the particles are bosons then an exchange of two particles is represented by an identity operator: the wave function is invariant and we say that the particles obey Bose statistics. If the particles are fermions then an exchange is represented by multiplication by (-1) : the wave function changes sign and we say that the particles obey Fermi statistics.

In one dimension the exchange of particles causes them inevitably to collide. Thus if the wave function changes sign when two identical particles are exchanged, we could say that the particles are noninteracting fermions, but we could as well say that the particles are interacting bosons such that the sign change is induced by the interaction as the particles pass one another.

Thus, identical-particle statistics is a rather tame concept in three (or more) spatial dimensions and also in one dimension. But in between these two cases, in two dimensions, a remarkably rich variety of types of particle statistics is possible. Apart from bosonic and fermionic behaviors, arbitrary phase factor or even non-trivial unitary evolutions can be obtained when two particles are exchanged [27]. Particles with such an exotic behavior were named *anyons* by Frank Wilczek.

The study of anyons started as a theoretical construction of two dimensional models [28]. It was soon realized that they can be encountered in physical systems with effective two dimensional behavior. Even in our three dimensional world, a two dimensional gas of electrons can be realized by trapping the electrons in a thin layer between two slabs of semiconductor, so that at low energies the electron motion in the direction perpendicular to the layer is

frozen out. In the presence of sufficiently strong magnetic field and low temperature these confined electron gases give rise to the *fractional quantum Hall effect* [29, 30]. The low energy excitations of these systems are localized quasiparticles that can actually exhibit anyonic statistics.

Systems that support anyons are called topological as their properties depend on global characteristics and not on local details. In the nineties it was argued that anyons could be employed to perform *quantum computation* [31].

Quantum computation requires the encoding of quantum information into qubits (two level quantum systems) and its manipulation with quantum gates (unitary operators acting on qubits). Errors, however, are present in any physical realization of quantum computation, coming from the environment or from control imperfection. Shor [32] and Steane [33] independently demonstrated that for sufficiently isolated quantum systems and for sufficiently precise quantum gates, *quantum error correction* can allow fault-tolerant quantum computation. However, the required limits demand a large overhead in qubits and quantum gates.

In contrast to this, anyonic quantum computation promises to solve the problem of errors from the hardware level. It was demonstrated by Kitaev [34] that a system of non-Abelian anyons with suitable properties can indeed be used to perform fault-tolerant quantum computation. The robustness against errors comes from the topological nature of the system.

3.1 Anyons as flux-charge composites

Let us take a closer look at the origin of anyons and their properties. First, let us recall the *Aharonov-Bohm effect* [35]: If an electric charge q is adiabatically transported along a path γ (counterclockwise) around a magnetic flux Φ , the wave function of the charge acquires a *topological phase* $e^{iq\Phi}$ (we are using the units with $c = \hbar = 1$), where

$$\Phi = \oint_{\gamma} \mathbf{A} \cdot d\mathbf{l} = \int \int_S (\nabla \times \mathbf{A}) \cdot d\mathbf{s} = \int \int_S \mathbf{B} \cdot d\mathbf{s} . \quad (3.1)$$

Here \mathbf{B} is the magnetic field, \mathbf{A} its vector potential and S is a surface enclosed by the path γ .

The word "topological" means that the Aharonov-Bohm phase is robust when we deform the trajectory of the charged particle — all that matters is the "winding number" of the charge about the flux. Note that in order to acquire a non-zero Aharonov-Bohm phase, the electric charge q doesn't even need to visit the region where $B \neq 0$, i.e. q is influenced by the vector potential \mathbf{A} itself. This marvelous result of Aharonov and Bohm totally changed the understanding of the role of the potential \mathbf{A} (and in general of the four-potential A^μ) in physics — rather than a mathematical construct it became a physical quantity.

To visualize the behavior of anyons one should think of them as being two dimensional composite particles consisting of a magnetic flux Φ confined inside an impenetrable circular

wall and an electric charge q stuck to the outside of the wall (or ring in two dimensions).¹

What happens if we perform an exchange of two of our flux-charge composite objects in a counterclockwise sense? Each charge q is adiabatically transported half way around the flux Φ of the other object. Thus each charge will acquire an Aharonov-Bohm phase that is, for symmetry reasons, exactly half of the phase generated by a complete revolution of the charge about the flux. Adding together the phases arising from the transport of both charges, we find that the exchange of the two flux-charge composites changes their wave function by the phase

$$\exp \left[i \left(\frac{1}{2} q \Phi + \frac{1}{2} q \Phi \right) \right] = e^{iq\Phi} \equiv e^{i\theta} . \quad (3.2)$$

The phase θ , generated when the two objects are exchanged, matches the phase generated when one of the two objects is rotated by 2π . In the latter case the charge q takes one full spin around the flux Φ , thus acquiring the Aharonov-Bohm phase $e^{iq\Phi}$.

The exchange statistics of our flux-charge composite particles is described by the angle $\theta \in [0, 2\pi)$. We refer to such particles as *Abelian anyons*. If the charges and fluxes, when exchanged, generate a unitary matrix instead of a mere phase factor then the particles are called *non-Abelian anyons*. In reality, the presence of charge and flux come from effective emerging gauge theory that describes the low energy behavior of the model [36].

3.2 Ising anyonic model

In our study of anyonic quantum walks we will be concerned with the Ising anyonic model with three particle types: 1 (vacuum), σ and ψ . These can be thought of as conserved quantum numbers (charges) of the particles. The fusion rules

$$\sigma \times \sigma = 1 + \psi , \quad \sigma \times \psi = \sigma , \quad \psi \times \psi = 1 , \quad (3.3)$$

$$\sigma \times 1 = \sigma , \quad \psi \times 1 = \psi , \quad 1 \times 1 = 1 \quad (3.4)$$

specify the possible values of the charge that can be obtained when two particles of known charges are combined together, or, read backwards, specify the possible ways for a charge to be split into two parts.² Note that 1, σ and ψ are labels, not vector spaces. Thus \times and $+$ are not the signs for tensor product and direct sum, respectively. Rather, fusion rules (3.3) and (3.4) should be regarded as abstract relations on the label set $\{1, \sigma, \psi\}$. For example, the first rule in (3.3) could also be written as $\{(\sigma, \sigma; 1), (\sigma, \sigma; \psi)\}$. The relation $\{(a, b; c)\}$ is symmetric in a and b , i.e. $a \times b = b \times a$. Physically, the fusion rules (3.3) signify that if we bring together two σ anyons, they are either fused to 1 (vacuum), i.e. annihilate (i.e. σ is its

¹In three dimensions one may envision a plane intersecting a magnetic solenoid directed perpendicular to the plane.

²These fusion rules are the fusion rules of the $SU(2)_2$ Chern-Simons theory. In fact, all anyonic models with no more than four particle types are closely related to the models that are found in the Chern-Simons theory.

own antiparticle), or they give rise to ψ (i.e. there are two fusion channels); σ and ψ give σ ; and ψ with ψ fuse to the vacuum. According to the rules (3.4) the vacuum 1 fuses trivially with all particles. Since $\sigma \times \sigma$ has two possible fusion channels, our anyonic model is called *non-Abelian*. If there were no fusion rule with more than one possible outcome, the model would be called *Abelian*. (General anyonic model is pedagogically introduced in [26].)

Assume that one creates from the vacuum a pair of anyons (σ, σ) (this is allowed by the first fusion rule in (3.3)). The state of these anyons can be denoted as $|\sigma, \sigma \rightarrow 1\rangle$ indicating that if we fuse back these anyons, their fusion outcome is known to be 1 due to the conservation of total charge. In general, when two arbitrary anyons are fused, it is possible to have various outcomes depending on their total state. In particular, for two σ anyons whose fusion results in ψ we define the state $|\sigma, \sigma \rightarrow \psi\rangle$. We also represent these states diagrammatically – Fig. 3.1. The two distinguishable orthonormal (by definition) states $|\sigma, \sigma \rightarrow 1\rangle$ and $|\sigma, \sigma \rightarrow \psi\rangle$

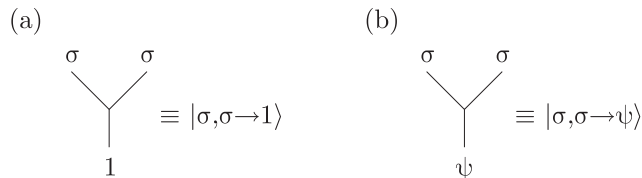


Figure 3.1: The diagrammatic representation of the states in the topological Hilbert space of a pair of σ anyons. (a) The fusion outcome is 1, (b) the fusion outcome is ψ .

span a two dimensional Hilbert space. This space is often called the "topological Hilbert space" of the pair of anyons (σ, σ) to emphasize that the quantum information encoded in a state from this space is encoded non-locally — it is a collective property of the pair (σ, σ) , not localized on either particle. Therefore the information is not vulnerable to decoherence due to local interactions with the environment.

When two particles undergo a counterclockwise exchange, their total charge c is unchanged. Therefore the state $|a, b \rightarrow c\rangle$ (in our case $a, b, c \in \{1, \psi, \sigma\}$) remains unchanged up to a phase factor R_{ab}^c — Fig. 3.2(a). We refer to R_{ab}^c as to the R -matrix.

We assume that fusion is associative, i.e.

$$(a \times b) \times c = a \times (b \times c), \quad a, b, c \in \{1, \psi, \sigma\}. \quad (3.5)$$

Mathematically, this is an axiom satisfied by the fusion rules of an anyonic model. Physically, it is imposed because the total charge of a system of three particles ought not to depend on whether we first fuse the first and the second particle and then fuse the result with the third one, or first fuse the second and the third particle and the result with the first one. Therefore, when three particles are fused to yield a total charge d , there are two natural ways to decompose the topological Hilbert space (or fusion space) V_{abc}^d of the three particles in

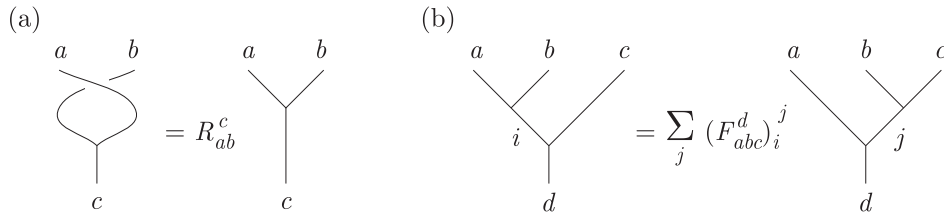


Figure 3.2: (a) The definition of the R -matrix. When particles a and b with fusion outcome c are exchanged (in a counterclockwise sense) the state $|a, b \rightarrow c\rangle$ acquires a phase R_{ab}^c . (b) The definition of the F -matrix. The two different ways of fusing three particles are connected through a unitary transformation F_{abc}^d .

terms of the fusion spaces of pairs of particles:

$$V_{abc}^d = \bigoplus_e |a, b \rightarrow e\rangle \otimes |e, c \rightarrow d\rangle = \bigoplus_f |a, f \rightarrow d\rangle \otimes |b, c \rightarrow f\rangle. \quad (3.6)$$

The two natural orthonormal bases of V_{abc}^d arising from this decomposition are related by a unitary transformation F_{abc}^d — the F -matrix (Fig. 3.2(b)).

For describing a system of many anyons it is convenient to adopt a *standard basis* for their topological Hilbert space. Suppose that $2n$ anyons³ of type σ are arranged sequentially along a line. Let the convention be that we first fuse the leftmost anyon with the second leftmost, the result of their fusing with the third anyon from the left and so on (Fig. 3.3). Notice that every even fusion outcome in this fusion chain is fixed by the fusion rules (3.3) and (3.4) to be σ , i.e. the dimension of the fusion space $\mathcal{H}_{fusion}^{(2n)}$ of $2n$ σ anyons is 2^{n-1} (total charge is also fixed). When *two* σ anyons are added to the system, the dimension of the fusion space raises by a factor of 2. Therefore one says that the *quantum dimension* of type σ anyons in our Ising model is $\sqrt{2}$.

Of course, the basis is chosen arbitrarily. If we preferred, we could imagine fusing the particles in a different order, and would obtain a different basis that could be expressed in terms of our standard one with a help from the F -matrix.

It is possible to access the fusion space by braiding the particles' world lines, i.e. by exchanging the positions of the particles. It suffices to say how exchanges of neighboring particles are represented; that is, to specify the action of the generators of the braid group. So far, we have discussed only the action of the braid group on a pair of particles with definite total charge (the R -matrix), which is not itself enough to tell us its action on the standard bases, because the two particles don't have a direct fusion channel in the standard basis (except for the first two particles from the left).

³We specialize to an even number of anyons because of the further applications in our anyonic quantum walk protocol.

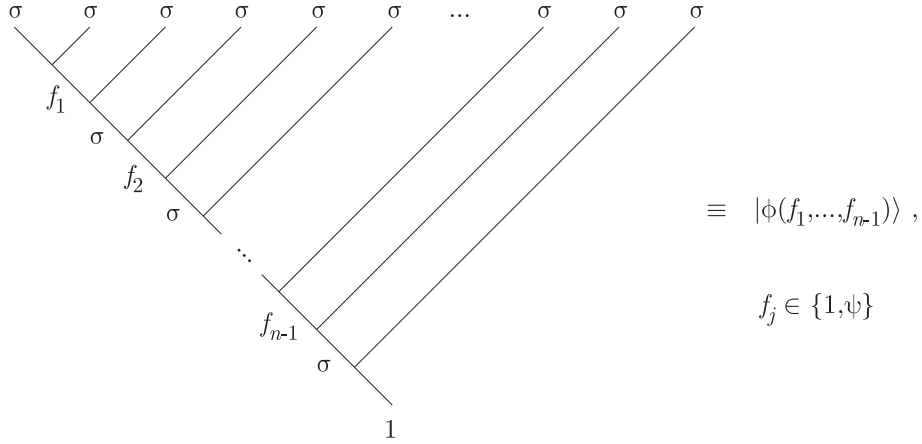


Figure 3.3: A vector of the standard basis of the topological Hilbert space of $2n$ σ anyons, $\mathcal{H}_{fusion}^{(2n)}$. The freedom of choosing independently $n - 1$ parameters $f_j \in \{1, \psi\}$ translates in the dimension of $\mathcal{H}_{fusion}^{(2n)}$ being 2^{n-1} .

Let us observe that by applying the F -matrix, we can move from the standard basis to the basis in which the R -matrix is block diagonal, apply R , and then apply F^{-1} to return back to the standard basis. The composition of these three operations, which expresses the effect of braiding on the standard basis, is denoted B (see Fig. 3.4).

The R and F (and consequently B) matrices are highly constrained by algebraic consistency conditions called the *pentagon and hexagon identities* (Fig. 3.5).

The pentagon identity involves the F -matrices only:

$$(F_{12c}^5)_a^d (F_{a34}^5)_b^c = \sum_e (F_{234}^d)_e^c (F_{1e4}^5)_b^d (F_{123}^b)_a^e ; \quad (3.7)$$

whereas the hexagon identity relates both F and R matrices:

$$R_{13}^c (F_{213}^4)_a^c R_{12}^a = \sum_b (F_{231}^4)_b^c R_{1b}^4 (F_{123}^4)_a^b . \quad (3.8)$$

There exists a theorem, which says that no other conditions need to be imposed to ensure the consistency between braiding (the R -matrices) and fusing (the F -matrices).

To obtain the R and F matrices for our Ising anyonic model (defined by the fusion rules (3.3) and (3.4)), one needs to solve the equations (3.7) and (3.8).⁴ Let us use the reference [1] to write the R and F matrices (in the basis $\{1, \psi\}$) that will be relevant for our anyonic quantum walk with Ising anyons:

$$R_{\sigma\sigma} \equiv \text{diag}(R_{\sigma\sigma}^1, R_{\sigma\sigma}^\psi) = \begin{pmatrix} 1 & 0 \\ 0 & i \end{pmatrix} , \quad (3.9)$$

⁴There are also alternative approaches [37].

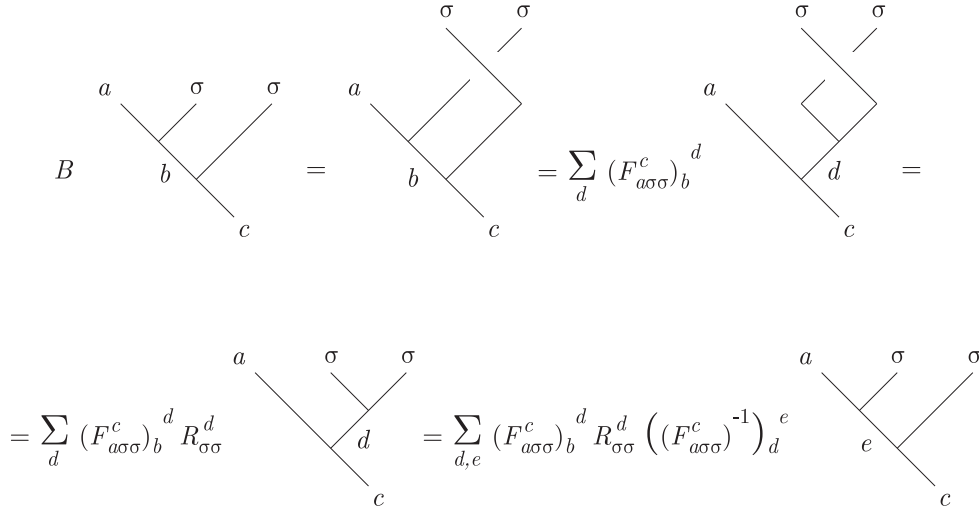


Figure 3.4: The braiding B of two particles that don't have a direct fusion channel can be expressed as a composition of three operations — F , R and F^{-1} .

$$F_{\sigma\sigma\sigma}^\sigma = \frac{1}{\sqrt{2}} \begin{pmatrix} 1 & 1 \\ 1 & -1 \end{pmatrix}. \quad (3.10)$$

The other relevant F -matrices (i.e. the rules that relate different bases of the fusion space) are trivially determined by the fusion rules (3.3) and (3.4).

Now we can finally write the B -matrices to find what happens when two neighboring σ anyons are exchanged (i.e. their worldlines are braided). Suppose there are $2n$ σ anyons arranged in line and their fusion state is described by a vector (or a superposition of vectors) $|\phi(f_1, \dots, f_{n-1})\rangle \in \mathcal{H}_{fusion}^{(2n)}$ (recall the Fig. 3.3). The braiding of the anyons j and $j+1$ (Fig. 3.6), denoted B_j , is represented by a linear operator on $\mathcal{H}_{fusion}^{(2n)} \simeq (\text{span}_{\mathbb{C}}\{1, \psi\})^{\otimes(n-1)} \simeq (\mathbb{C}^2)^{\otimes(n-1)}$.

Regarding the figures 3.3 and 3.6, we can see that the indices a, b, c in Fig. 3.6 may either take the form

$$(a, b, c) = (\sigma, f, \sigma), \quad f \in \{1, \psi\} \quad (3.11)$$

for j even or

$$(a, b, c) = (f, \sigma, f'), \quad f, f' \in \{1, \psi\} \quad (3.12)$$

for j odd. By employing the procedure described by Fig. 3.4 and expressions (3.9) and (3.10), we obtain the results for B_j 's, where $2 \leq j \leq 2n-1$,⁵

$$B_{2k} = \underbrace{\mathbf{1} \otimes \dots \otimes \mathbf{1}}_{k-1} \otimes B \otimes \underbrace{\mathbf{1} \otimes \dots \otimes \mathbf{1}}_{n-1-(k-1)-1} \quad (3.13)$$

⁵ $j=1$ is a special marginal case which we shall not encounter during the anyonic quantum walk studied in the next chapter.

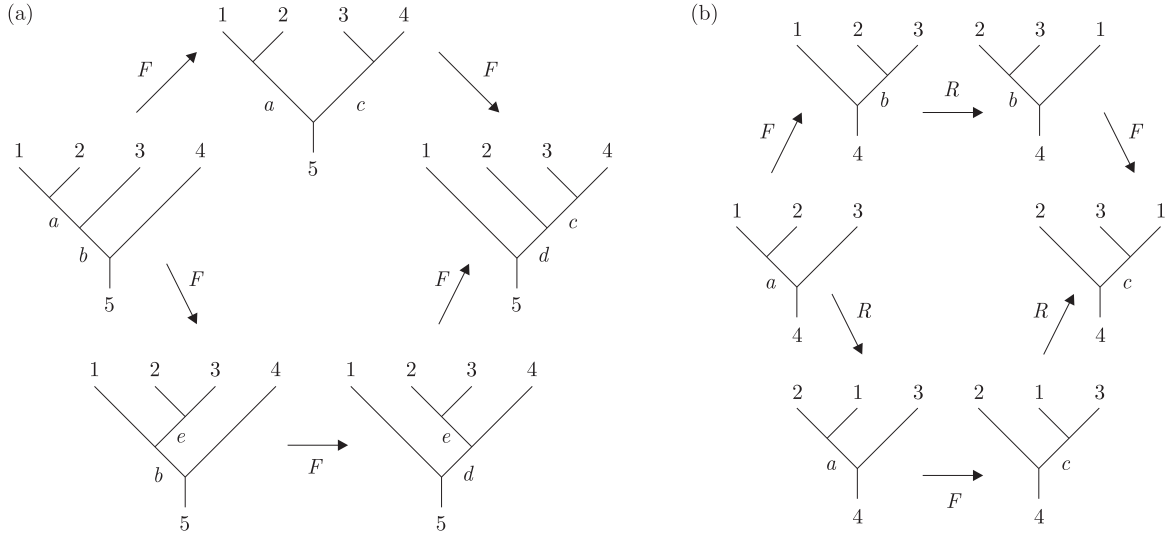


Figure 3.5: (a) The pentagon identity and (b) the hexagon identity are algebraic consistency conditions that an anyonic model must satisfy. They can be used to find the F and R matrices of the model.

and

$$B_{2k+1} = \underbrace{\mathbb{1} \otimes \dots \otimes \mathbb{1}}_{k-1} \otimes A \otimes \underbrace{\mathbb{1} \otimes \dots \otimes \mathbb{1}}_{n-1-(k-1)-2}, \quad (3.14)$$

where $\mathbb{1}$ is the identity matrix 2×2 ,

$$B = F_{\sigma\sigma\sigma}^{\sigma} R_{\sigma\sigma} (F_{\sigma\sigma\sigma}^{\sigma})^{-1} = \frac{e^{i\frac{\pi}{4}}}{\sqrt{2}} \begin{pmatrix} 1 & -i \\ -i & 1 \end{pmatrix} \quad (3.15)$$

and

$$A = \begin{pmatrix} 1 & 0 & 0 & 0 \\ 0 & i & 0 & 0 \\ 0 & 0 & i & 0 \\ 0 & 0 & 0 & 1 \end{pmatrix} = \frac{e^{i\frac{\pi}{4}}}{\sqrt{2}} (\mathbb{1} \otimes \mathbb{1} - i\sigma_3 \otimes \sigma_3), \quad \sigma_3 = \begin{pmatrix} 1 & 0 \\ 0 & -1 \end{pmatrix}. \quad (3.16)$$

To find the matrix A one needs to substitute into the diagram Fig. 3.4: $b = \sigma$ and $(a, c) = (1, 1), (1, \psi), (\psi, 1)$ and (ψ, ψ) .

The matrices B_j form a representation of the braid group of $2n$ strands presented in the section 2.2. This representation is not faithful as

$$B_j^4 = \mathbb{1}. \quad (3.17)$$

Notice that the B_j 's are indeed unitary, i.e. $B_j^{-1} = B_j^\dagger$.

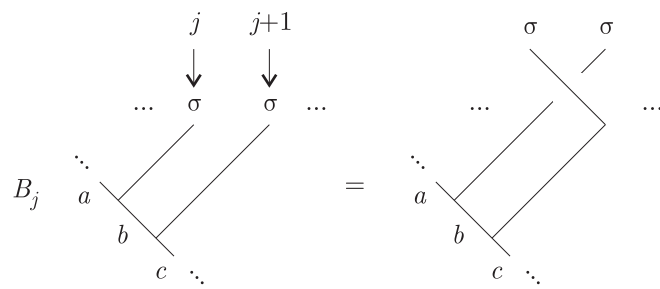


Figure 3.6: The braiding operation B_j swaps (in a counterclockwise manner) the particles on positions j and $j + 1$.

Chapter 4

Anyonic quantum walk on a line

Quantum walks have been studied in both the continuous time [38] and discrete time [39] versions. We briefly describe the discrete time quantum walk on the infinite line, which will be later generalized to the anyonic case. It is defined in direct analogy with a *classical random walk*.

4.1 Classical random walk

In the classical discrete random walk, a particle (the walker) is located at one of a set of definite positions (we will consider a set of integers on the line). In response to a random event — for example, the flipping of a coin — the particle moves either right or left.¹ This process is iterated and the motion of the particle is analyzed statistically. These systems provide good models for diffusion of particles in a fluid (the Brownian motion), the motion of vacancies in a crystal and for other stochastic processes.

Denote the probability to find the walker after t steps at site s by $P_t(s)$. The time evolution of $P_t(s)$ is described by the recursion equation

$$P_{t+1}(s) = \frac{1}{2} \left(P_t(s-1) + P_t(s+1) \right), \quad s \in \mathbb{Z}. \quad (4.1)$$

For a walker starting at the origin at time $t = 0$ the recursion (4.1) has the solution

$$P_t(s) = \frac{1}{2^t} \binom{t}{\frac{t+s}{2}}, \quad t \geq 0, \quad s \in \mathbb{Z}, \quad (4.2)$$

where we use the convention that the binomial coefficient $\binom{n}{k}$ is nonzero only if n and k are nonnegative integers such that $n \geq k$. Note that at even times only the even sites can be occupied, while at odd times only the odd sites can be occupied. The distributions $P_t(s)$ for various times t are plotted in Fig. 4.1 and one can see that they spread in time.

¹We will consider, for simplicity, the probability $\frac{1}{2}$ to move in either direction

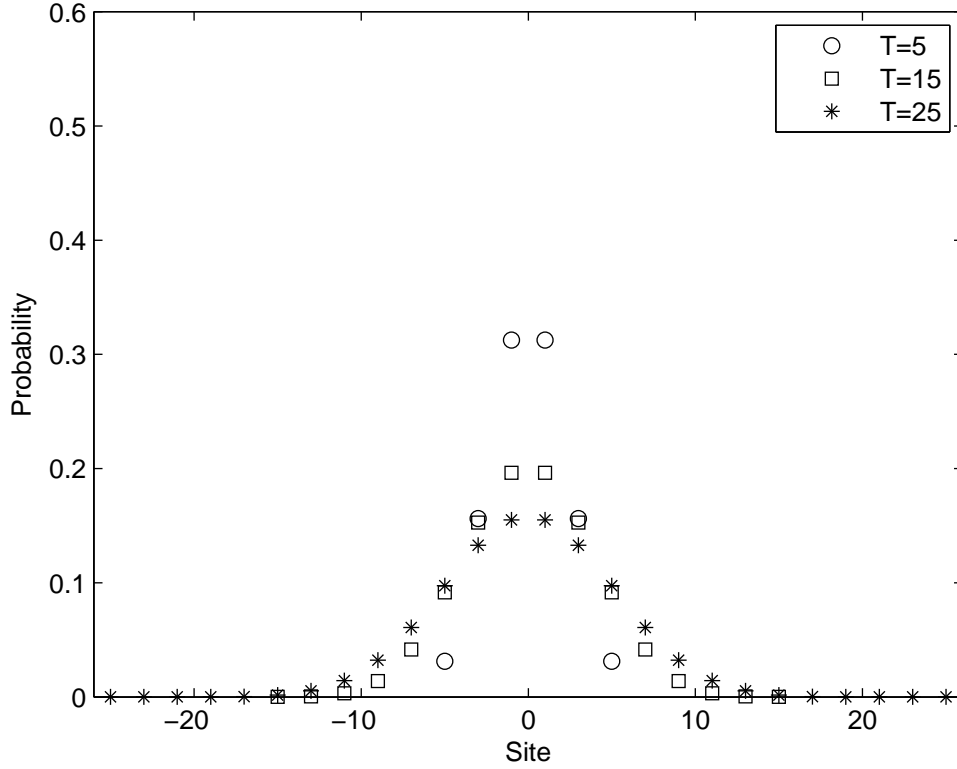


Figure 4.1: The position probability distribution $P_T(s)$ of a classical random walker on an infinite line at the times $T = 5, 15$ and 25 . The variance of the distribution grows linearly in time.

This spreading can be quantified by the time evolution of the variance

$$\sigma^2(t) = \langle s^2 \rangle (t) - \langle s \rangle^2 (t) \quad (4.3)$$

of the probability distributions $P_t(s)$, where

$$\langle s \rangle (t) = \sum_s s P_t(s) , \quad (4.4)$$

$$\langle s^2 \rangle (t) = \sum_s s^2 P_t(s) \quad (4.5)$$

are the first and the second moment, respectively, of $P_t(s)$. It is straightforward to calculate that in our case of a classical random walk on line

$$\langle s \rangle_{RW} (t) = 0 , \quad (4.6)$$

$$\langle s^2 \rangle_{RW} (t) = t \quad (4.7)$$

and so

$$\sigma_{RW}^2(t) = t. \quad (4.8)$$

4.2 Quantum walk on a line

To make a quantum analogy of the random walk discussed above one commonly proceeds as follows. We denote the basis states for the quantum walk as ordered pairs of labels $|s\rangle_{space} \otimes |c\rangle_{coin} \equiv |s\rangle|c\rangle$, where $s \in \mathbb{Z}$ is the position and $c \in \{0, 1\}$ is the spin-like state of the coin. The state of the walker is described by the wave function $|\Phi\rangle \in \mathcal{H} = \text{span}\{|s\rangle|c\rangle\}_{s \in \mathbb{Z}, c \in \{0, 1\}}$.

One step of the quantum walk is given by a unitary operator \hat{W} acting on \mathcal{H} . \hat{W} is defined as

$$\hat{W} = (\hat{S}^\dagger \otimes |0\rangle\langle 0| + \hat{S} \otimes |1\rangle\langle 1|)(\hat{I} \otimes \hat{U}), \quad (4.9)$$

where \hat{I} is the identity operator on $\mathcal{H}_{space} = \text{span}\{|s\rangle\}_{s \in \mathbb{Z}}$, \hat{S} and \hat{S}^\dagger are unitary shift operators acting on \mathcal{H}_{space} in the following way

$$\hat{S}|s\rangle = |s+1\rangle, \quad \hat{S}^\dagger|s\rangle = |s-1\rangle \quad (4.10)$$

and \hat{U} is a unitary "coin flipping" operator acting on the two dimensional Hilbert space $\mathcal{H}_{coin} = \text{span}\{|0\rangle, |1\rangle\}$, chosen for the sake of simplicity

$$\hat{U} = \frac{1}{\sqrt{2}} \begin{pmatrix} 1 & 1 \\ 1 & -1 \end{pmatrix}. \quad (4.11)$$

Starting from the initial state $|\Phi(0)\rangle = |0\rangle \otimes |c_0\rangle$ and applying t times the operator \hat{W} , we obtain the state

$$|\Phi(t)\rangle = \hat{W}^t |\Phi(0)\rangle. \quad (4.12)$$

Ultimately, we are interested in the probability distribution $P_t(s)$ of the spatial location, s , of the walker after t steps. For this purpose we trace out the coin degree of freedom to obtain the reduced density matrix

$$\rho_{space}(t) = \text{Tr}_{coin}(|\Phi(t)\rangle\langle\Phi(t)|) \quad (4.13)$$

and calculate the expectation values of position measurements

$$P_t(s) = \text{Tr}\left(|s\rangle\langle s| \rho_{space}(t)\right) = \langle s | \rho_{space}(t) | s \rangle. \quad (4.14)$$

As the walk progresses, quantum interference occurs whenever there is more than one possible path of t steps that leads to the same position. This interference is both constructive and destructive, which causes some probabilities to be amplified or decreased at each time step. This leads to the different behavior compare to the classical random walk (plots for the initial state $|\Phi(0)\rangle = |0\rangle \otimes |0\rangle$ are given in Fig. 4.2). In the classical random walk there

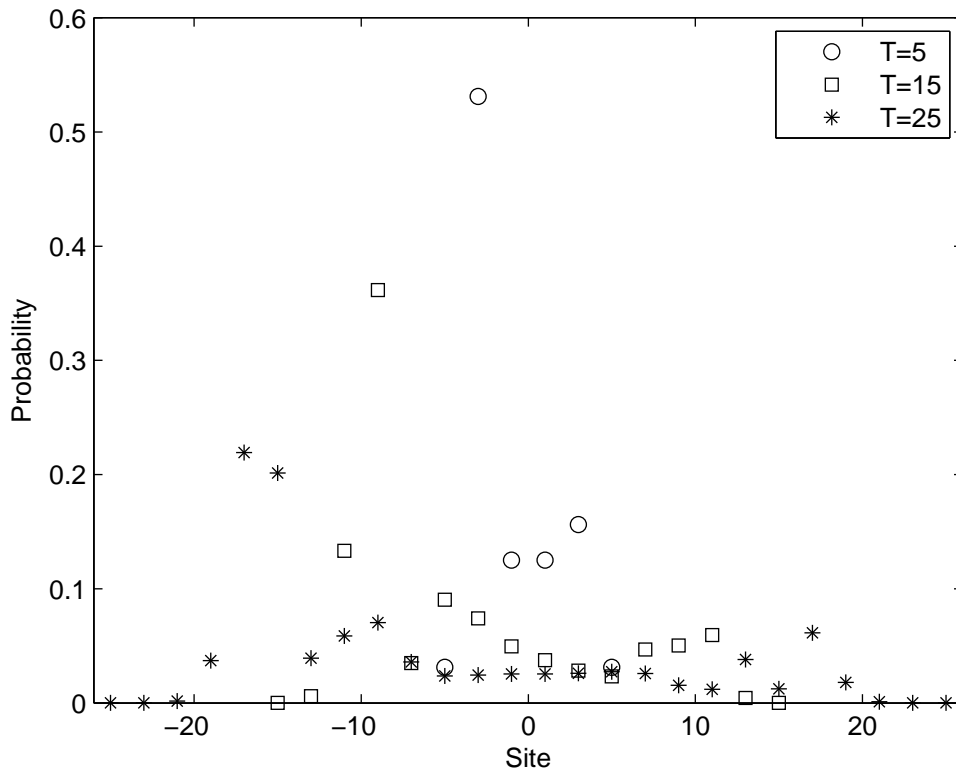


Figure 4.2: The position probability distribution $P_T(s)$ of a quantum walker on an infinite line at the times $T = 5, 15$ and 25 . The distribution is not symmetric, it rather has an evident left drift, which is a consequence of the choice of \hat{U} and $|c_0\rangle$. The variance of the distribution grows quadratically in time.

is only one path (particle history) being realized at a time whereas in the quantum walk all possible particle histories are realized simultaneously, which causes them to interfere.

Quantum walks are often studied numerically as it proves hard to give a closed formula for $|\Phi(t)\rangle$ and $P_t(s)$. Some analytic approximative results have been obtained though [39]. An important difference between the classical random walks on line and the quantum walks on line is in the rate of spreading characterized by the variance $\sigma^2(t)$. Unlike in the case of the classical random walk, where in general $\sigma_{RW}^2 \sim t$, the variance of the quantum walk grows quadratically:

$$\sigma_{QW}^2 \sim t^2. \quad (4.15)$$

This quadratic speedup can be employed to perform certain computational tasks faster using so called *quantum algorithms*. Some famous examples are Grover's database search algorithm [41] and Shor's integer factorization algorithm [42].

4.3 A walk with Ising anyons

In order to reveal the statistics of anyons in a quantum walk, we consider a single anyonic walker, denoted w , braiding around other anyons (labeled by an integer index j) which stay in fixed positions. The anyons involved are all of the same type σ . We use the Ising anyonic model described in Sec. 3.2, i.e. our anyons are *non-Abelian*.² The anyons are created in pairs from the vacuum and placed in a canonical order in the plane with position (space between two adjacent static anyons) labeled by an integer s , as seen in Fig. 4.3(a).

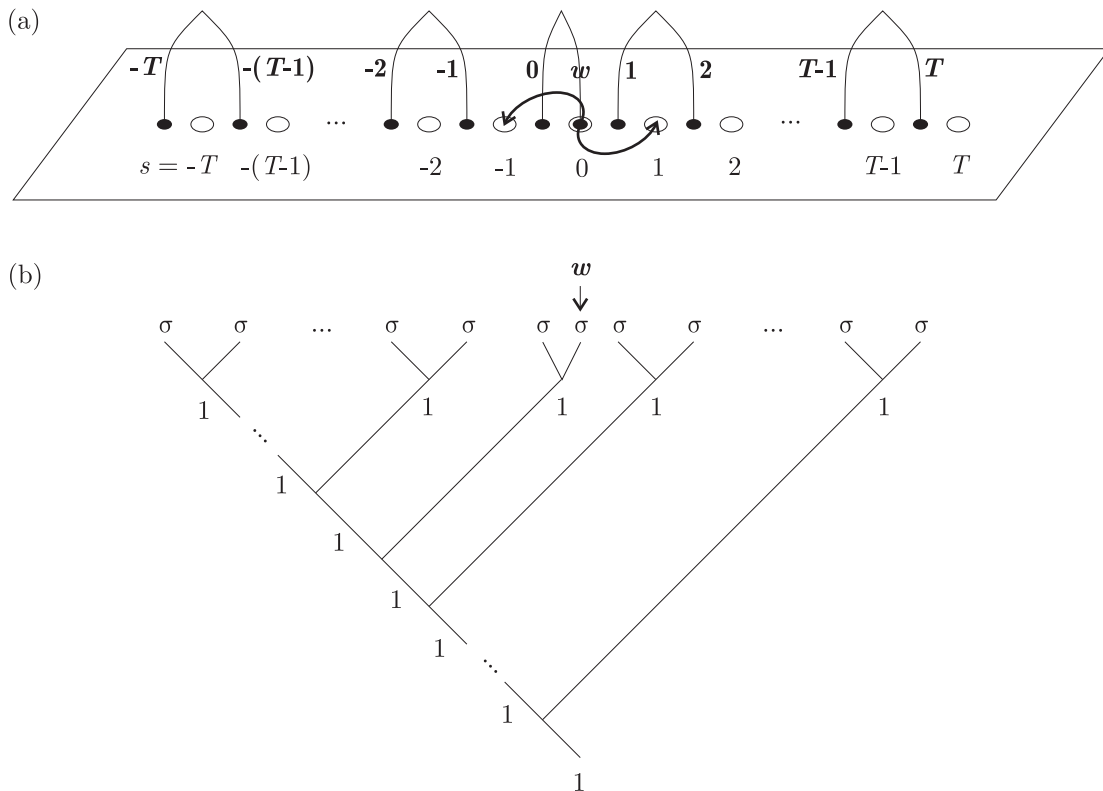


Figure 4.3: (a) The anyons, which are free to move in the plane, are placed in line and labeled from left to right by an index j . The walker, denoted w , occupies positions labeled by an integer s (the j -th anyon is situated between the positions $j - 1$ and j). We show the case for which T , the maximum number of steps, is even. The case when T is odd differs only very slightly. (b) The initial fusion state of the walk — σ anyons are created from the vacuum in pairs.

The initial state in the fusion space is depicted in Fig. 4.3(b). Employing the F -matrices (in fact, here it suffices to use just the fusion rules of the Ising model (3.3) and (3.4)), the

²The Abelian case is discussed in [1]. The variance of the walk can be probed analytically and it behaves qualitatively the same as in the usual quantum walk (see section 4.2 in [1]), i.e. grows quadratically in the number of steps.

expression of the initial fusion state in the standard basis is found to be

$$|\phi_{in}\rangle = |\phi(\underbrace{1, \dots, 1}_{n-1})\rangle. \quad (4.16)$$

The number of created anyons, $2n$, defines the maximum number of steps, T , that the walker can perform without reaching the boundary points. To perform a T -step walk, we assume a creation of $n = 2\lceil \frac{T}{2} \rceil + 1$ pairs of anyons ($\lceil x \rceil$ is the ceiling function).

The walker moves to the left or to the right by always braiding in the *anticlockwise* sense with its neighboring anyons (again Fig. 4.3(a)). This can be achieved by employing only one coin (which has two degrees of freedom). One can show that the braidwords (the sequences of the elements of the braid group) that result from this quantum walk have the same computational power as arbitrary braidwords (i.e. the case when one allows both clockwise and anticlockwise braiding). Recall the relation (3.17) which implies $B_j^{-1} = B_j^3$. Thus, braidings equivalent to clockwise moves can be produced given enough anticlockwise ones. Notably, fixing the chirality of the braiding means that Abelian sectors of any physical theory will not contribute to the walker's distribution since all walking paths accumulate the same overall phase. Hence the protocol with only anticlockwise braidings probes the truly non-Abelian statistics.

The Hilbert space of our system is

$$\mathcal{H}^{(T)} = \mathcal{H}_{space}^{(T)} \otimes \mathcal{H}_{coin} \otimes \mathcal{H}_{fusion}^{(2n)}, \quad (4.17)$$

where T is the maximum number of steps and $2n$ is the number of anyons.³ $\mathcal{H}_{space}^{(T)} = \text{span}\{|s\rangle\}_{s=-T}^T$ describes the spatial position of the walker and $\mathcal{H}_{coin} = \text{span}\{|0\rangle, |1\rangle\}$ carries the information about the coin outcome, which dictates the walker to move left or right and braid anticlockwise with its left or right neighbour, respectively. The local degrees of freedom of the other anyons, while measurable, will be conserved during this walk and will be ignored.

When the walker braids around a static anyon j , the action on the fusion space $\mathcal{H}_{fusion}^{(2n)}$ is represented by a unitary operator B_j . The matrices B_j , $j = 0, \pm 1, \pm 2, \dots$, are the ones derived in Section 3.2 and given by the expressions (3.13-3.16). Only, the index j is shifted in such a way that B_0 of the anyonic quantum walk corresponds to B_n given by (3.14).

One step of the anyonic quantum walk is given by a unitary operator \hat{W} acting on $\mathcal{H}^{(T)}$. The definition of \hat{W} is analogous to the quantum walk case (compare with (4.9)), but more complicated for we need to incorporate, in addition, the fusion space with braiding operations which are position dependent. Thus

$$\hat{W} = \sum_s (\hat{S}^\dagger \otimes |0\rangle\langle 0| \otimes B_s + \hat{S} \otimes |1\rangle\langle 1| \otimes B_{s+1}) (\hat{I} \otimes \hat{U} \otimes \hat{I}) (|s\rangle\langle s| \otimes \hat{I} \otimes \hat{I}), \quad (4.18)$$

³Although T must be specified before starting the walk in order to create appropriate (finite) number of anyons, this is no actual limitation as T can be chosen arbitrarily large.

where the sum is taken over all positions, \hat{S} and \hat{S}^\dagger are defined by (4.10) and the coin operator \hat{U} is chosen to be the same as in the quantum walk case (4.11), i.e. $\hat{U} = \frac{1}{\sqrt{2}} \begin{pmatrix} 1 & 1 \\ 1 & -1 \end{pmatrix}$.

Let the initial state of our anyonic quantum walk be

$$|\Phi(0)\rangle = |0\rangle \otimes |0\rangle \otimes |\phi_{in}\rangle \quad (4.19)$$

with $|\phi_{in}\rangle$ as in (4.16). After t steps of the walk ($t < T$), $|\Phi(0)\rangle$ evolves to

$$|\Phi(t)\rangle = \hat{W}^t |\Phi(0)\rangle = \sum_{\vec{a} \in \{0,1\}^t} |s_{\vec{a}}\rangle \otimes (|a_t\rangle \langle a_t| \hat{U} |a_{t-1}\rangle \dots \langle a_2| \hat{U} |a_1\rangle \langle a_1| \hat{U} |0\rangle) \otimes B_{\vec{a}} |\phi_{in}\rangle, \quad (4.20)$$

where the sum runs over all bitstrings $\vec{a} = (a_1, \dots, a_t)$ of the length t , i.e. over all possible histories of the walker. Naturally, $a_i = 0$ means "step to the left" and $a_i = 1$ "step to the right". We denoted $s_{\vec{a}}$ the final position of the history \vec{a} , i.e.

$$s_{\vec{a}} = (\text{number of 1's in } \vec{a}) - (\text{number of 0's in } \vec{a}). \quad (4.21)$$

Finally, we denoted $B_{\vec{a}}$ the braidword coming from the history \vec{a} . $B_{\vec{a}}$ is nonlocal since, while building it up, we need to keep track of the position: if the walker is located at the position s and steps left (right), the braidword gains the matrix B_s (B_{s+1}) respectively. Hence

$$B_{\vec{a}} \equiv \prod_{i=1}^t B_{s_{(a_1, \dots, a_{i-1})} + a_i}. \quad (4.22)$$

For example, for $t = 6$ and the history $\vec{a} = (1, 1, 0, 0, 0, 0)$, we obtain the braidword $B_{\vec{a}} = B_{-1} B_0 B_1 B_2 B_2 B_1$.⁴

Since we chose the coin flipping operator conveniently, we can write the coin part of the history \vec{a} as

$$|a_t\rangle \langle a_t| \hat{U} |a_{t-1}\rangle \dots \langle a_2| \hat{U} |a_1\rangle \langle a_1| \hat{U} |0\rangle = \left(\frac{1}{\sqrt{2}} \right)^t (-1)^{z(\vec{a})} |a_t\rangle, \quad (4.23)$$

where the newly introduced function $z(\vec{a})$, which counts the number of pairs of adjacent 1's in the bitstring \vec{a} , can be written as

$$z(\vec{a}) = \sum_{i=1}^{t-1} a_i a_{i+1}. \quad (4.24)$$

The density matrix $\rho(t)$ corresponding to the state $|\Phi(t)\rangle$ then reads

$$\rho(t) = \sum_{\vec{a}, \vec{a}' \in \{0,1\}^t} |s_{\vec{a}}\rangle \langle s_{\vec{a}'}| \otimes \frac{1}{2^t} (-1)^{z(\vec{a}) + z(\vec{a}')} |a_t\rangle \langle a'_t| \otimes (B_{\vec{a}} |\phi_{in}\rangle \langle \phi_{in}| B_{\vec{a}'}^\dagger). \quad (4.25)$$

⁴Note that we read the vectors \vec{a} in the usual way from left to right, whereas the braidwords, being compositions of matrices (mappings), are to be read from right to left.

We would like to know the position distribution of the walker regardless of the coin and anyonic states. For that we need to trace the coin space and the fusion space of anyons, resulting in

$$\mathrm{Tr}_{\mathrm{coin}} \mathrm{Tr}_{\mathrm{fusion}} \rho(t) = \sum_{\vec{a}, \vec{a}' \in \{0,1\}^t} |s_{\vec{a}}\rangle \langle s_{\vec{a}'}| \frac{1}{2^t} (-1)^{z(\vec{a})+z(\vec{a}')} \underbrace{\langle a'_t | a_t \rangle}_{\delta_{a_t, a'_t}} \langle \phi_{in} | B_{\vec{a}'}^\dagger B_{\vec{a}} | \phi_{in} \rangle, \quad (4.26)$$

and calculate the expectation values of the position measurement, yielding the position distribution after t steps

$$P_t(s) = \langle s | \mathrm{Tr}_{\mathrm{coin}} \mathrm{Tr}_{\mathrm{fusion}} \rho(t) | s \rangle = \frac{1}{2^t} \sum_{\substack{\vec{a}, \vec{a}' \in \{0,1\}^t \\ a_t = a'_t \\ |\vec{a}| = |\vec{a}'| = H(t,s)}} (-1)^{z(\vec{a})+z(\vec{a}')} \langle \phi_{in} | B_{\vec{a}'}^\dagger B_{\vec{a}} | \phi_{in} \rangle. \quad (4.27)$$

The function $|\vec{a}|$, commonly called the *Hamming weight*, returns the number of 1's in the bitstring \vec{a} . All bitstrings ending after t steps at the same position s have the same Hamming weight

$$H(t, s) = \frac{t + s}{2}. \quad (4.28)$$

In (4.27) we sum over all pairs of histories of the walker (we will call these pairs *paths*) which satisfy certain constraints. We introduce the set

$$\mathcal{P}_{t,s} \equiv \{(\vec{a}, \vec{a}') \mid \vec{a}, \vec{a}' \in \{0,1\}^t, a_t = a'_t, |\vec{a}| = |\vec{a}'| = H(t, s)\} \quad (4.29)$$

of all paths that are involved in the sum in (4.27). Each path $(\vec{a}, \vec{a}') \in \mathcal{P}_{t,s}$ is weighted by the phase factor

$$(-1)^{z(\vec{a})+z(\vec{a}')} \langle \phi_{in} | B_{\vec{a}'}^\dagger B_{\vec{a}} | \phi_{in} \rangle \quad (4.30)$$

and the whole sum in (4.27) is normalized by the factor $\frac{1}{2^t}$. While the coin trace contribution $(-1)^{z(\vec{a})+z(\vec{a}')}$ is rather straightforward to calculate, care needs to be taken when one takes the trace over anyonic degrees of freedom (i.e. the fusion space) with the contribution $\langle \phi_{in} | B_{\vec{a}'}^\dagger B_{\vec{a}} | \phi_{in} \rangle$.

4.3.1 Evaluation of the trace over the fusion space

In principle, we could use our knowledge of the braid matrices B_j . They are given (up to the shifting of the index j , as discussed earlier) by the expressions (3.13-3.16). Calculating $\langle \phi_{in} | B_{\vec{a}'}^\dagger B_{\vec{a}} | \phi_{in} \rangle$ then involves only matrix multiplications. This is easy to explain, but rather hard and time-consuming to carry out (even for a computer). At this point, the knot theory comes onto the stage. We will use the results presented in [43] and discussed in [1] to make a connection between the trace over the fusion space and the Jones polynomial and other phenomena in the knot theory.

Our goal is to calculate

$$\langle \phi_{in} | B_{\vec{a}'}^\dagger B_{\vec{a}} | \phi_{in} \rangle = \text{Tr} \left(| \phi_{in} \rangle \langle \phi_{in} | B_{\vec{a}'}^\dagger B_{\vec{a}} \right) \quad (4.31)$$

for a given path (\vec{a}, \vec{a}') . It is useful to represent (\vec{a}, \vec{a}') pictorially as suggested in Fig. 4.4. It can be shown [43] that the trace (4.31) corresponds to the Markov closure (introduced in

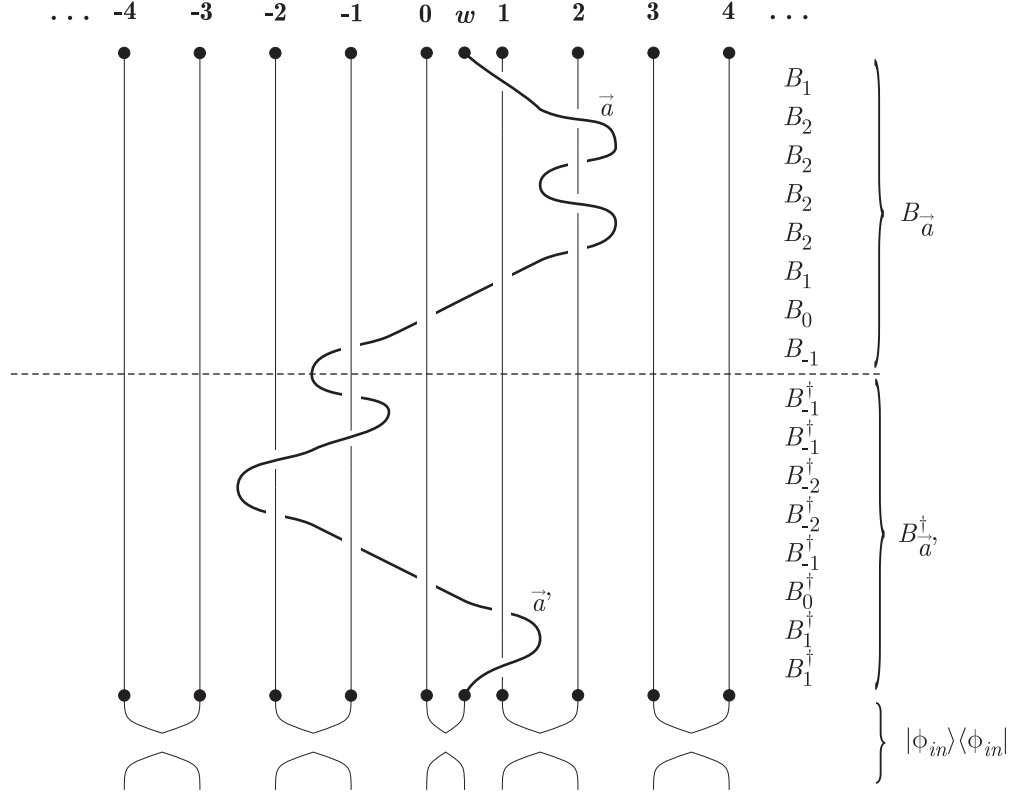


Figure 4.4: A diagrammatic representation of the expression $| \phi_{in} \rangle \langle \phi_{in} | B_{\vec{a}'}^\dagger B_{\vec{a}}$ arising from a generic path (\vec{a}, \vec{a}') . After taking the trace over the fusion space this diagram changes to Fig. 4.5(a).

Section 2.2, Fig. 2.11(a)) of the braid diagram on Fig. 4.4, which is, in fact, the Plat closure (introduced in Section 2.2, Fig. 2.11(b)) of the braid $B_{\vec{a}'}^\dagger B_{\vec{a}}$ (as depicted in Fig. 4.5(a)). The statement is

$$\text{Tr} \left(| \phi_{in} \rangle \langle \phi_{in} | B_{\vec{a}'}^\dagger B_{\vec{a}} \right) = \frac{1}{d^{n-1}} \left\langle \left(B_{\vec{a}'}^\dagger B_{\vec{a}} \right)^{Plat} \right\rangle (A), \quad (4.32)$$

where n is the number of pairs of anyons, $\langle \cdot \rangle$ denotes the Kauffman bracket (recall the definition (2.14-2.16)) and d is related to the Kauffman bracket variable A as $d = -A^{-2} - A^2$. For the Ising anyonic model (which is derived from the Chern-Simons theory with gauge group $SU(2)_2$) $A = ie^{-i\frac{\pi}{8}}$ and so $d = \sqrt{2}$.

From Fig. 4.5(a) it is evident that the writhe $w(L)$ (defined by (2.17)) of the link $L \equiv \left(B_{\vec{a}'}^\dagger B_{\vec{a}} \right)^{Plat}$ is equal to 0, as for any path (\vec{a}, \vec{a}') the number of positive crossings is the same

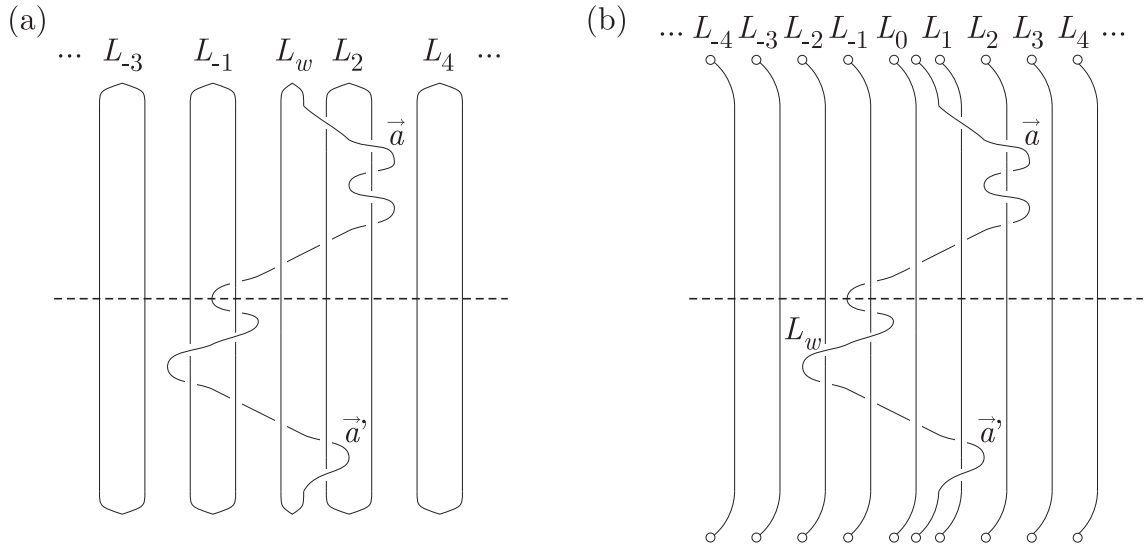


Figure 4.5: Tracing of the diagram in Fig. 4.4 produces the link depicted in (a). It corresponds to the Plat closure of the braid $B_{\vec{a}}^\dagger B_{\vec{a}}$. In the modified protocol the tracing produces the link (b) that is the Markov closure of the braid $B_{\vec{a}}^\dagger B_{\vec{a}}$. In (b), the little circles on the top and the bottom of the diagram mean that the two endpoints of each strand are identified, glued together.

as the number of negative crossings. It is therefore easier to relate the Kauffman bracket and the Jones polynomial of the link L . The relation (2.18) simplifies to

$$V_L(t) = V_L(A^{-4}) = \langle L \rangle (A) . \quad (4.33)$$

We conclude that

$$\text{Tr} \left(|\phi_{in}\rangle \langle \phi_{in}| B_{\vec{a}}^\dagger B_{\vec{a}} \right) = \langle \phi_{in}| B_{\vec{a}}^\dagger B_{\vec{a}} |\phi_{in}\rangle = \frac{1}{d^{n-1}} V_L(A^{-4}) = \frac{1}{(\sqrt{2})^{n-1}} V_L(i) . \quad (4.34)$$

You might object that we are calculating the Jones polynomial of a link without specifying its orientation. However, as discussed in Section 2.3, the orientation of L is regarded in $V_L(t)$ only through the writhe of L . Since, in our case, $w(L) = 0$, all orientations yield the same result for $V_L(t)$.

At the special value $t = i$, the Jones polynomial of a link can be related to a simpler knot invariant known as the *Arf invariant*, which takes values only in the set $\{0, 1\}$. The *arf* of a knot K , which is a single component link, is equal to zero if K is *pass equivalent*⁵ to the unknot (Fig. 2.1) and is equal to one if K is pass equivalent to the trefoil knot (Fig. 2.2).

⁵Pass equivalency of two knots is defined similarly as equivalency of knot diagrams. Besides the Reidemeister moves, one is allowed to also use so called *pass moves* (see [15] for the definition and more details on this topic). Of course, pass equivalent knots, in general, are not the same knots.

The *arf* can be related to the *Alexander polynomial* Δ_K (definition of which is given, for example, in [16]), which can be computed in time polynomial in the number of crossings of a braid presentation of the knot [44]. We are dealing with multicomponent links, for which *arf* has a more complicated definition in terms of a knot that is related to the link [45]. In [46] Murakami showed that

$$V_L(i) = \begin{cases} (\sqrt{2})^{\#(L)-1}(-1)^{arf(L)} & \text{if } L \text{ is proper} \\ 0 & \text{if } L \text{ is not proper,} \end{cases} \quad (4.35)$$

where $\#(L)$ is the number of components in the link L , and an oriented link L is said to be proper if for each link component L_k (in the case of Fig. 4.5(a) $k \in \{\dots, -3, -1, w, 2, 4, \dots\}$)

$$\sum_{j \neq k} lk(L_k, L_j) \text{ is even,} \quad (4.36)$$

where the linking number $lk(., .)$ has been defined earlier — (2.1). For the links that arise from the anyonic walk the number of link components $\#(L)$ is equal to the number of initialized pairs of anyons n . Therefore (4.34) becomes

$$\langle \phi_{in} | B_{\bar{a}'}^\dagger B_{\bar{a}} | \phi_{in} \rangle = \begin{cases} (-1)^{arf(L)} & \text{if } L \text{ is proper} \\ 0 & \text{if } L \text{ is not proper.} \end{cases} \quad (4.37)$$

A link L is said to be *totally proper* if for all pairs of link components

$$lk(L_k, L_j) \text{ is even.} \quad (4.38)$$

The quantity $arf(L)$ can be expressed in a rather convenient way provided that L is totally proper [45]:

$$arf(L) = \left(\sum_i arf(L_i) + \frac{1}{4} \sum_{i < j} (\lambda(L_i, L_j) + lk(L_i, L_j)) + \sum_{i < j < k} \tau(L_i, L_j, L_k) \right) \text{ mod } 2, \quad (4.39)$$

where $arf(L_i)$ is the *arf* of the knot L_i , λ is the unoriented Sato-Levine invariant and τ is the Milnor triple point invariant. Roughly speaking, the Sato-Levine invariant counts the number of Whitehead links (Fig. 2.4(c)) for a pair of components and the Milnor triple counts the number of Borromean rings (Fig. 2.4(b)) in a triple of components [45].

The formula (4.39) becomes particularly useful if we consider a modified anyonic quantum walker protocol where, in order to perform a T -step walk, we start with $2n$ pairs of anyons ($n = 2\lceil \frac{T}{2} \rceil + 1$), braid all right members of each pair to the right uniformly via the braid word B , and then perform the walk just on the $2n$ strands corresponding to these right members (we have already seen this procedure in Section 2.2, Fig. 2.12). That is, we transform the initial state $|\phi(1, \dots, 1)\rangle$ into $B|\phi(1, \dots, 1)\rangle$. The links that we get from this modified protocol are of the form

$$L = \left(B^\dagger B_{\bar{a}'}^\dagger B_{\bar{a}} B \right)^{Plat} = \left(B_{\bar{a}'}^\dagger B_{\bar{a}} \right)^{Markov}, \quad (4.40)$$

i.e. the braids we obtain are the same as before the modification, but the closure has changed from Plat to Markov (Fig. 4.5). We denote the set of links coming from the new protocol by

$$\overline{\mathcal{P}}_{t,s} \equiv \left\{ \left(B_{\vec{a}'}^\dagger B_{\vec{a}} \right)^{Markov} \mid (\vec{a}, \vec{a}') \in \mathcal{P}_{t,s} \right\}. \quad (4.41)$$

It is easy to see that all links $L \in \overline{\mathcal{P}}_{t,s}$ (for any t and s) that are proper, are also totally proper. (The condition (4.36) gives 0 for $k = w$ and "lk(L_k, L_w) is even" otherwise.) Since there is no self-linking of the components of L , $arf(L_i) = 0 \forall i$. The total linking number $\sum_{i < j} lk(L_i, L_j) = \sum_j lk(L_w, L_j) = 0$. Finally, $\lambda(L_i, L_j) = 0 \forall i, j$, because any pair of link components L_i, L_j can be viewed as a link that arises from a 2-strand braid through the Markov closure and one can show that at least 3 strands are needed to produce the Whitehead link.⁶ Putting these facts together, we can simplify the expression for $arf(L)$ (4.39):

$$arf(L) = \sum_{i < j < k} \tau(L_i, L_j, L_k) \pmod{2}. \quad (4.42)$$

4.3.2 Numerical calculation

We are interested in the spatial distribution $P_t(s)$ of the walker after t steps. We will use the modified protocol. First, let us denote

$$\mathcal{P}_{t,s}^{(prop)} \equiv \left\{ (\vec{a}, \vec{a}') \in \mathcal{P}_{t,s} \mid \left(B_{\vec{a}'}^\dagger B_{\vec{a}} \right)^{Markov} \text{ is proper} \right\} \quad (4.43)$$

the set of proper links arising from the paths in $\mathcal{P}_{t,s}$. Due to (4.37) and (4.42) the formula (4.27) reads

$$P_t(s) = \frac{1}{2^t} \sum_{(\vec{a}, \vec{a}') \in \mathcal{P}_{t,s}^{(prop)}} (-1)^{z(\vec{a}, \vec{a}') + \tau(\vec{a}, \vec{a}')}, \quad (4.44)$$

where we denoted, for brevity, $z(\vec{a}, \vec{a}') \equiv z(\vec{a}) + z(\vec{a}')$ (the coin contribution to the phase) and $\tau(\vec{a}, \vec{a}') \equiv \sum_{i < j < k} \tau(L_i, L_j, L_k) \pmod{2}$, where $L = \left(B_{\vec{a}'}^\dagger B_{\vec{a}} \right)^{Markov}$ (the fusion degree of freedom contribution).

The computer programme that computes $P_t(s)$ proceeds as follows:

- For given number of steps t and position s , sum over all paths $(\vec{a}, \vec{a}') \in \mathcal{P}_{t,s}$.
- Find whether the link $L = \left(B_{\vec{a}'}^\dagger B_{\vec{a}} \right)^{Markov}$ is proper or not. For this purpose compute the linking numbers $lk(L_j, L_w)$, where L_w is the walker's component of L and j runs over all the other components. If there exists j such that $lk(L_j, L_w)$ is an odd number, add zero to the overall sum and take another path. Otherwise:
- Compute $z(\vec{a}, \vec{a}') \equiv z(\vec{a}) + z(\vec{a}')$ using the formula (4.24).

⁶Using 2 strands, the only possible braids are of the form b_1^k , where $k \in \mathbb{Z}$.

- Compute $\tau(\vec{a}, \vec{a}') \equiv \sum_{i < j < k} \tau(L_i, L_j, L_k) \pmod{2}$. Notice that $\tau(L_i, L_j, L_k) = 0$ if none of the indices i, j, k is w . If, for instance, $j = w$, take the braidword $(B_{\vec{a}'}^\dagger B_{\vec{a}})^{Markov}$ and omit, for the moment, all braid generators B_l that don't cause L_w link with either L_i or L_k . We are left with two braid generators (let's denote them B_p, B_q), which we can represent by two 2×2 matrices.⁷ The computation of $\tau(L_i, L_w, L_k)$ is then only a question of multiplication of matrices (or rather a use of their anti-commutation relations). Calculate also the other cases — $\tau(L_w, L_j, L_k)$ and $\tau(L_i, L_j, L_w)$ — and return $\tau(\vec{a}, \vec{a}')$.
- Add $(-1)^{z(\vec{a}, \vec{a}') + \tau(\vec{a}, \vec{a}')}$ to the overall sum and take another path and repeat.

The results of the numerical calculation up to 25 time steps are presented in figures 4.6 and 4.7.

The position distribution of the anyonic quantum walk with Ising anyons resembles the position distribution of a classical random walk (Fig. 4.1). It doesn't have the typical quantum walk side peaks (Fig. 4.2). The plot of the variance of the anyonic walk and its comparison to the classical and quantum cases confirms that the anyonic walk seems to lose the quadratic speed-up of ordinary quantum walk. Rather, its variance seems to approach the classical linear behavior.

⁷The matrices

$$B_p = \begin{pmatrix} 1 & 0 \\ 0 & i \end{pmatrix}, \quad B_q = \frac{e^{i\frac{\pi}{4}}}{\sqrt{2}} \begin{pmatrix} 1 & -i \\ -i & 1 \end{pmatrix}$$

will do the job. A nice feature is that $B_p^2 = \sigma_3$ and $B_q^2 = \sigma_1$.

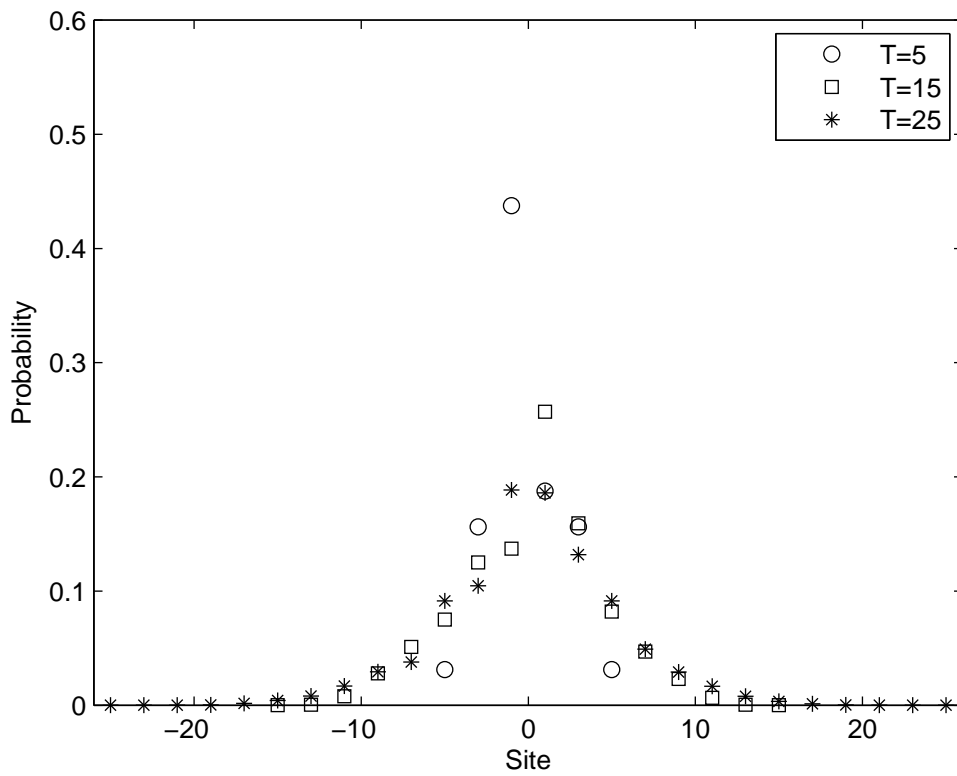


Figure 4.6: The position distribution of the Ising anyonic walker after 5, 15 and 25 time steps. It resembles more the "bell" shape of the classical walker distribution Fig. 4.1 than the quantum walker distribution Fig. 4.2.

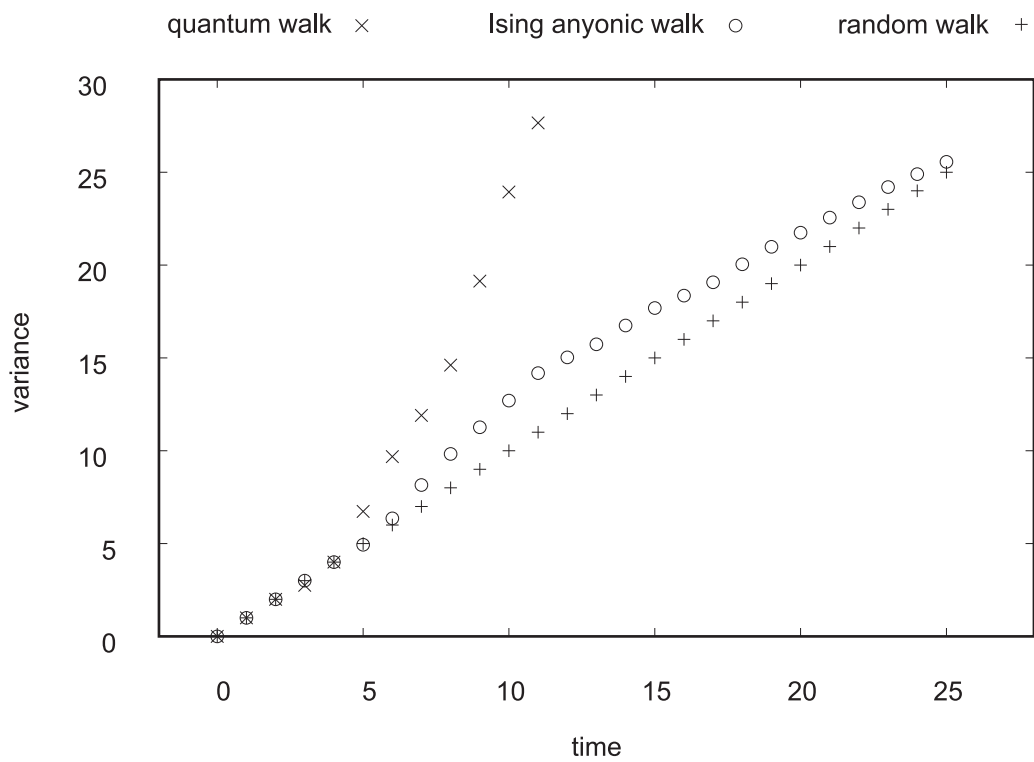


Figure 4.7: Comparison of the time evolution of variances of the Ising anyonic walk, the classical random walk and the quantum walk. The anyonic walk approaches the classical one. The data, however, are available up to 25 time steps only.

Chapter 5

Conclusion, discussion and outlook

We studied the quantum walk on a line with anyons. We used the non-Abelian anyons described by the Ising anyonic model derived from the $SU(2)$ level 2 Chern-Simons theory. We saw that the nontrivial exchange statistics of the particles affects strikingly the position distribution $P_t(s)$ of the walker (Fig. 4.6) — it resembles the classical random walk distribution rather than the quantum walk distribution.

We used some knot theoretical results to simplify the expression for $P_t(s)$, however, we were not able to provide a closed analytical formula. That's why we wrote a computer programme and approached the problem numerically, obtaining the position distribution $P_t(s)$ up to 25 time steps. Since the complexity of the programme is exponential in the number of steps t (the scaling seems to be roughly like 4^t) the barrier of 25 steps is hard to overcome.

From $P_t(s)$ we calculated the variance of the Ising anyonic walker. The comparison with the classical and the quantum walk variance (Fig. 4.7) confirmed that the non-Abelian Ising walker behaves classically (talking about the spreading of its position distribution) unlike in the case of an Abelian anyonic walker, which behaves qualitatively same as an ordinary quantum walker [1]. The support for the statement "Ising walk becomes classical" comes from the numerics. It is hard to give a good and persuading theoretical reasoning.

5.1 Why the Ising walk behaves classically

We can view the Ising walk as a "deformation" of the usual quantum walk (the quantum walk with trivial exchange statistics of particles). The fusion degree of freedom, represented in the position distribution sum (4.27) by the expression (4.37), causes the quantum walk contributions $(-1)^{z(\vec{a}, \vec{a}')} to get multiplied by$

- 0 if the link $L = \left(B_{\vec{a}'}^\dagger B_{\vec{a}} \right)^{Markov}$ is not proper,
- 1 if L is proper and $arf(L) = 0$ or
- -1 if L is proper and $arf(L) = 1$.

If all our links were proper and $\text{arf}(L)$ was always zero, we would get the usual quantum walk distributions (Fig. 4.2). What we do observe is, however, much more complicated.

Let us define the set $\mathcal{P}_{t,s}^{(mirror)} \equiv \{(\vec{a}, \vec{a}') \in \mathcal{P}_{t,s} \mid \vec{a} = \vec{a}'\}$. We shall call the paths from $\mathcal{P}_{t,s}^{(mirror)}$ the *mirror paths*. It is easy to see that all the links arising from the mirror paths are proper with arf equal to zero (note that $B_{\vec{a}}^\dagger B_{\vec{a}} = \mathbb{1}$) and that $(-1)^{z(\vec{a}, \vec{a})} = (-1)^{z(\vec{a})+z(\vec{a})} = 1$. Therefore we divide (4.44) into two terms:

$$P_t(s) = \underbrace{\frac{1}{2t} \sum_{(\vec{a}, \vec{a}') \in \mathcal{P}_{t,s}^{(mirror)}} 1}_{P_t^{(RW)}(s)} + \underbrace{\frac{1}{2t} \sum_{(\vec{a}, \vec{a}') \in \mathcal{P}_{t,s}^{(prop)} \setminus \mathcal{P}_{t,s}^{(mirror)}} (-1)^{z(\vec{a}, \vec{a}') + \tau(\vec{a}, \vec{a}')}}_{P_t^{(ERR)}(s)}. \quad (5.1)$$

The first term, $P_t^{(RW)}(s)$, is the classical walk distribution, for the cardinality of the set $\mathcal{P}_{t,s}^{(mirror)}$ is equal to the number of histories \vec{a} leading after t steps to the site s . The second term, $P_t^{(ERR)}(s)$, is the difference between the Ising walk and the classical walk.¹ When one plugs (5.1) into the formula for variance (4.3), one finds that for a convenient large- t behavior of $P_t^{(ERR)}(s)$, the variance of the Ising walk approaches the classical linear relation (4.8). More specifically (we will not do a detailed derivation though), we need to assume that

- the coin contribution $(-1)^{z(\vec{a}, \vec{a}')}$ and the fusion space contribution $(-1)^{\tau(\vec{a}, \vec{a}')}$ are not correlated (or at least that their correlation can be neglected), i.e. if a path (\vec{a}, \vec{a}') is such that $(-1)^{\tau(\vec{a}, \vec{a}')} = 0, -1$ or $+1$, respectively, then $(-1)^{z(\vec{a}, \vec{a}')}$ is equally likely to be $+1$ or -1 ; and that
- the ratio $\frac{|\mathcal{P}_{t,s}^{(prop)} \setminus \mathcal{P}_{t,s}^{(mirror)}|}{|\mathcal{P}_{t,s} \setminus \mathcal{P}_{t,s}^{(mirror)}|}$ of the amount of non-mirror paths constituting a proper link over all non-mirror paths drops off as t goes to infinity fast enough (at least like $\frac{1}{t^2}$).

The first assumption seems plausible, because of the different nature of calculating $(-1)^{z(\vec{a}, \vec{a}')}$ and $(-1)^{\tau(\vec{a}, \vec{a}')}.$ ² The second assumption seems plausible, because for t increasing, the typical number of link components that the walker's component L_w links with grows and therefore it becomes less likely that all linking numbers happen to be even. Importantly, both assumptions are supported by the numerics. A more rigorous justification of these assumptions could be the base for a proof that the Ising walk variance is, for large t , linear in t .

5.2 Walks with $SU(2)$ level k anyons

As we have mentioned many times during this work, the Ising anyonic model has its origin in the $SU(2)_2$ Chern-Simons theory. If we take a general $SU(2)_k$ anyonic model ($k = 2, 3, 4, \dots, +\infty$), we get a family of walks labeled by k . The walks are different from the

¹Note that $\sum_s P_t^{(ERR)}(s) = 0$, i.e. $P_t^{(ERR)}(s)$ is not a probability distribution.

²Again, however, it is hard to tackle the problem rigorously.

Ising walk in the evaluation of the Kauffman bracket (4.32), where now $A = ie^{-\frac{\pi}{2(k+2)}}$ and $d = 2 \cos \frac{\pi}{k+2}$ [1]. The evaluation of a walk with general k becomes more complicated, because we can no longer express the Jones polynomial as the Arf invariant to simplify the calculations.

It can be shown that for $k = +\infty$ the anyonic walk becomes a standard quantum walk with the variance growing quadratically. We argued that for $k = 2$ the variance of the Ising walk (for a large number of steps) behaves classically, i.e. linearly. Between $k = 2$ and $k = +\infty$ we expect to observe "something in between", some transition. The nature of this transition is, at the moment, an open question.

Bibliography

- [1] G. K. Brennen, D. Ellinas, V. M. Kendon, J. K. Pachos, I. Tsohantjis and Z. Wang (2010), "Anyonic quantum walks", *Annals of Physics* **325**, 664; arXiv:0910.2974v1 [quant-ph]
- [2] N. Shevi, J. Kempe and K. B. Whaley (2003), *Phys. Rev. A* **67**, 052307
- [3] A. M. Childs, R. Cleve, E. Deotto, E. Farhi, S. Gutmann and D. A. Spielman (2003), *Proc. 35th Annual ACT STOC*, pp. 59
- [4] M. Mohseni, P. Rebentrost, S. Lloyd and A. Aspuru-Guzik (2008), *Jour. of Chem. Phys.* **129**, 174106
- [5] B. C. Travaglione and G. J. Milburn (2002), *Phys. Rev. A* **65**, 032310
- [6] W. Dür, R. Raussendorf, V. M. Kendon and H.-J. Briegel (2002), *Phys. Rev. A* **66**, 052319
- [7] B. C. Sanders, S. D. Bartlett, B. Tregenna and P. L. Knight (2003), *Phys. Rev. A* **67**, 042305
- [8] V. M. Kendon and B. C. Sanders (2004), *Phys. Rev. A* **71**, 022307
- [9] T. D. Mackay, S. D. Bartlett, L. T. Stephenson and B. C. Sanders (2002), *J. Phys. A: Math. Gen.* **35**, 2745
- [10] V. M. Kendon and B. Tregenna (2003), *Phys. Rev. A* **67**, 042315
- [11] A. Bracken, D. Ellinas and I. Smyrnakis (2007), *Phys. Rev. A* **75**, 022322; *Virtual Jour. Quant. Information* **7**, 3
- [12] D. Bouwmeester and I. Marzoli, G. P. Karman, W. Schleich and J. P. Woerdman (1999), *Phys. Rev. A* **61**, 013410
- [13] Y. Omar *et al.* (2006), *Phys. Rev. A* **74**, 042304
- [14] "Knot theory", Wikipedia, http://en.wikipedia.org/wiki/Knot_theory (27 April 2010, 17:07)

- [15] C. C. Adams (2004), "The Knot Book: An Elementary Introduction to the Mathematical Theory of Knots", American Mathematical Society
- [16] L. H. Kauffman (1987), "On Knots", Princeton
- [17] Hass, Joel (1998), "Algorithms for recognizing knots and 3-manifolds", Chaos, Solitons and Fractals (Elsevier) 9: 569581 arXiv:math/9712269
- [18] Rolfsen, Dale (1976), "Knots and Links", Publish or Perish
- [19] K. Reidemeister (1932), "Knotentheorie", Ergebnisse der Mathematik und ihrer Grenzgebiete (Alte Folge 0, Band 1, Helf 1), Berlin:Springer; (reprint Berlin:Springer-Verlag, 1974) (English transl.: L. Boron, C. Christenson and B. Smith (1983), BCS Associates, Moscow, Idaho)
- [20] V. F. R. Jones, "Hecke Algebra Representations of Braid Groups and Link Polynomials", The Annals of Mathematics, Second Series, Vol. 126, No. 2 (Sep., 1987), pp. 335-388
- [21] V. F. R. Jones (18 August 2005), Lecture notes: "The Jones Polynomial", <http://math.berkeley.edu/~vfr/>
- [22] V. F. R. Jones, "A polynomial invariant for knots via von Neumann algebras", Bull. Amer. Math. Soc. (N.S.) **12** (1985), 335-388
- [23] E. Artin (1947), "Theory of Braids", Ann. Math. **48**, 101-126
- [24] L. H. Kauffman, "State models and the Jones polynomial", Topology 26 (1987), no.3, 395-407
- [25] J. K. Pachos (2010), "Introduction to Topological Quantum Computation", lecture notes, University of Leeds
- [26] J. Preskill (14 June 2004), "Lecture Notes for Physics 219: Quantum Computation", California Institute of Technology
- [27] J. M. Leinaas and J. Myrheim (1977), Nuovo Cimento B **37**, 1
- [28] F. Wilczek (1982), Phys. Rev. Lett. **49**, 957
- [29] R. B. Laughlin (1983), Phys. Rev. Lett. **50**, 1395
- [30] F. E. Camino, W. Zhou and V. J. Goldman (2007), Phys. Rev. Lett. **98**, 076805
- [31] G. Castagnoli and M. Rasetti (1993), Int. J. of Mod. Phys. **32**, 2335
- [32] P. Shor (1995), Phys. Rev. A **52**, 2493

- [33] A. M. Steane (1996), Phys. Rev. Lett. **77**, 793
- [34] A. Kitaev (2003), Annals Phys. 303, 2
- [35] Y. Aharonov and D. Bohm (1959), Phys. Rev. **115**, 485
- [36] Z. Nussinov and G. Ortiz (2009), Proc. Nat. Ac. Sc. USA **106**, 16944
- [37] Z. Fan and H. de Garis (2009), "Braid matrices and quantum gates for Ising anyons topological quantum computation", The European Physical Journal B **74**, 419
- [38] E. Farhi and S. Gutmann (1998), Phys. Rev. A **58**, 915
- [39] A. Ambainis, E. Bach, A. Nayak, A. Vishwanath and J. Watrous (2001), Proc. 33rd Annual ACM STOC, pp.37; A. Nayak and A. Vishwanath, arXiv:quant-ph/0010117
- [40] T. A. Brun, H. A. Carteret and A. Ambainis (2003), Phys. Rev. Lett. **91**, 130602
- [41] L. K. Grover, (May 1996) "A fast quantum mechanical algorithm for database search", Proceedings, 28th Annual ACM Symposium on the Theory of Computing, p. 212
- [42] P. W. Shor (1997), "Polynomial-Time Algorithms for Prime Factorization and Discrete Logarithms on a Quantum Computer", SIAM J. Comput. 26 (5): 1484-1509, arXiv:quant-ph/9508027v2
- [43] D. Aharonov, V. Jones, Z. Landau (2006), "A Polynomial Quantum Algorithm for Approximating the Jones Polynomial", arXiv:quant-ph/0511096v2
- [44] J. W. Alexander (1928), Trans. Amer. Math. Soc. **2**, 30
- [45] R. Kirby and P. Melvin (2004), Geometry and Topology Monographs **7**, 213
- [46] H. Murakami (1986), J. Math. Soc. Japan **38**, 335